

Tectono-thermal evolution of the Maud Belt: New SHRIMP U–Pb zircon data from Gjelsvikfjella, Dronning Maud Land, East Antarctica

A. Bisnath^a, H.E. Frimmel^{a,*},¹, R.A. Armstrong^b, W.S. Board^a

^a *Department of Geological Sciences, University of Cape Town, Rondebosch 7701, South Africa*

^b *The Australian National University, Canberra, ACT 0200, Australia*

Received 27 April 2004; received in revised form 21 June 2006; accepted 26 June 2006

Abstract

The Maud Belt in Dronning Maud Land (western East Antarctic Craton) preserves a high-grade polyphase tectono-thermal history with two orogenic episodes of Mesoproterozoic (1.2–1.0 Ga) and Neoproterozoic (0.6–0.5 Ga) age. New SHRIMP U–Pb zircon data from southern Gjelsvikfjella in the northeastern part of the belt make it possible to differentiate between a series of magmatic and metamorphic events. The oldest event recorded is the formation of an extensive 1140–1130 Ma volcanic arc. This was followed by 1104 ± 8 Ma granitoids that might represent, together with so far undated mafic dykes, part of a decompression melting-related bimodal suite that reflects the sub-continental Umkondo igneous event. The first high-grade metamorphism is constrained at 1070 Ma. The metamorphic age data are similar to those obtained from other parts of the Maud Belt, but also from the Namaqua-Natal Belt in South Africa, but the preceding arc formation was diachronous in the two belts. This indicates that the two belts did not form a continuous volcanic arc unit as suggested in previous models, but became connected only at the end of the Mesoproterozoic.

Intense reworking during the Neoproterozoic, probably as a result of continent–continent collision between components of Gondwana, is indicated by ductile refoliation, further high-grade metamorphic recrystallisation and metamorphic zircon overgrowths at approximately 530 Ma. This was followed by late- to post-tectonic magmatism, reflected by 500 Ma granite bodies and 490 Ma aplite dykes as well as a 480 Ma gabbro body.

© 2006 Elsevier B.V. All rights reserved.

Keywords: Zircon geochronology; Gjelsvikfjella; Maud Belt; East Antarctica; Gondwana

1. Introduction

Dronning Maud Land in East Antarctica records useful information for the understanding of both the amal-

gamation and fragmentation of supercontinents, once towards the end of the Mesoproterozoic at ca. 1.2–1.0 Ga (equivalent to the ‘Grenvillian’ of North America) and again towards the late Neoproterozoic to Early Cambrian at ca. 0.6–0.5 Ga (the ‘Pan-African’ of Africa). The tectonic framework of East Antarctica is dominated by the East Antarctic Craton (Tingey, 1991; Krynanuw, 1996), fragments of Archaean continental crust (e.g. the Grunehogna Craton) surrounded by younger orogenic belts, such as the Maud Belt (Fig. 1). Rocks of the Maud Belt are exposed, from southwest to northeast, in the Heime-

* Corresponding author. Tel.: +49 931 888 5420; fax: +49 931 888 4620.

E-mail address: hartwig.frimmel@uni-wuerzburg.de (H.E. Frimmel).

¹ Present address: Institute of Mineralogy, University of Würzburg, Am Hubland, D-97074 Würzburg, Germany.

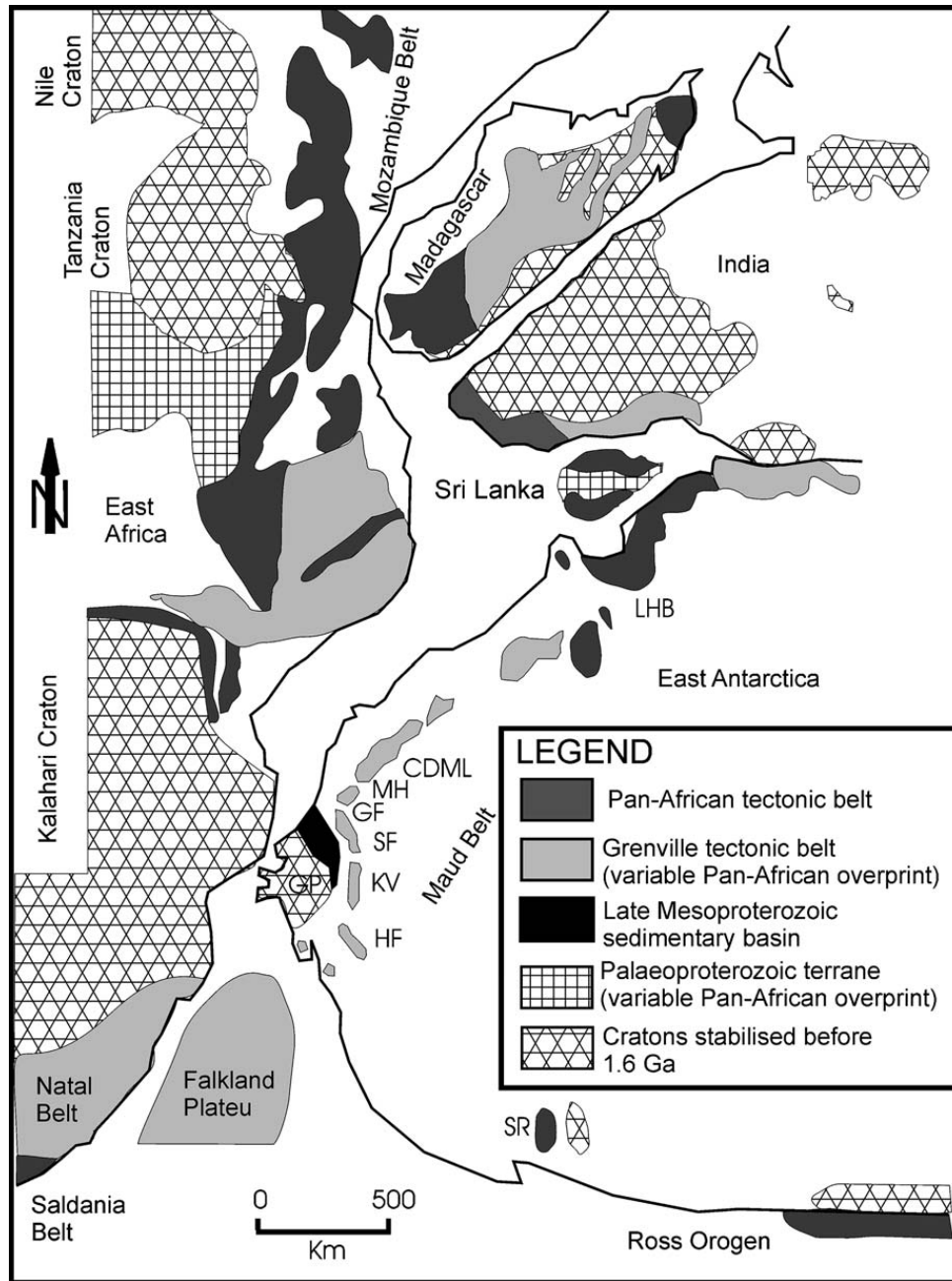


Fig. 1. Map showing correlations between Africa and East Antarctica within a Gondwana framework (after Reeves and de Wit, 2000; Frimmel, 2004). Abbreviations are: Heimfrontfjella (HF), Kirwanveggen (KV), H.U.Sverdrupfjella (SF), Gjelsvikfjella (GF), Mühlig-Hofmannfjella (MH), Central Dronning Maud Land (CDML), Lützow-Holm Bay (LHB), Shackleton Range (SR) and Grunehogna Craton (GC).

frontfjella, the Kirwanveggen, the H.U. Sverdrupfjella, the Gjelsvikfjella and western Mühlig-Hofmannfjella (Fig. 1). The belt is dominated by Mesoproterozoic supracrustal and intrusive rocks that were subsequently intruded by Neoproterozoic and Early Palaeozoic granitoids and mafic rocks (Arndt et al., 1991; Moyes and Groenewald, 1996; Jackson, 1999; Jacobs et al., 1999; Paulsson and Austrheim, 2003). In late Precambrian palaeogeographic reconstructions the Maud Belt is typically placed as part of the Kalahari Craton (e.g. Hoffman,

1991; Dalziel, 1997), which amalgamated with East Antarctica during the assembly of Gondwana at ca. 500 Ma (e.g. Meert, 2003; Collins and Pisarevsky, 2005).

The penetrative foliation in the Maud Belt has been suggested to be Mesoproterozoic in age (Groenewald et al., 1995; Grantham et al., 1995; Jackson, 1999) implying that the Maud Belt is a continuous tectonic belt not only from southwestern to central Dronning Maud Land but also beyond East Antarctica, linking up with the Namaqua-Natal Belt in South Africa. A growing num-

ber of geochronological data, however, point to major structural reworking of that Mesoproterozoic crust during Pan-African orogeny. A strong Pan-African thermal overprint and melt generation has been documented for central Dronning Maud Land, at 9° to 11° E and 72° to 71°40' (Jacobs et al., 1998), where a Pan-African age has been suggested for pervasive east–west trending structures (Jacobs et al., 2003a,b,d).

Further southwest in the Kirwanveggen area, the age of the regional pervasive, northeast-trending fabric is equivocal, because of possible co-linearity of the late Mesoproterozoic and late Neoproterozoic/Cambrian structures (Jackson, 1999). Recent U–Pb SHRIMP data on monazite inclusions in fabric-forming minerals from an intervening area in the H.U. Sverdrupfjella (Board et al., 2005) indicate a Pan-African age for a dominant top-to-northwest shear fabric there. These data challenge the existing geodynamic models that explain the Maud Belt as an essentially Mesoproterozoic tectonic belt that experienced only thermal overprinting during the Pan-African orogeny.

Gjelsvikfjella is situated in the western portion of central Dronning Maud Land (Fig. 1), at 2° to 5°35'E and 71°46' to 72°15'S, and lies east of the Jutulstraumen-Pencksøkket glacier. There the dominant northeasterly structural trend that defines the Maud Belt in western Dronning Maud Land changes to an easterly trend that marks central Dronning Maud Land. Thus, the outcrops of the Gjelsvikfjella provide the linkage between two extreme domains of the Maud Belt that followed different tectono-thermal evolutionary paths. Yet, so far little data has been available for this crucial sector of the Maud Belt.

The aim of this study is, therefore, to fill this gap in our understanding of the Maud Belt by providing new precise geochronological data on a variety of rock types that have been mapped in the area. It complements a detailed study of the metamorphic history (Bisnath and Frimmel, 2005) and of the geochemistry of various generations of (meta-) igneous rocks (Grosch et al., 2004). Some of the principal questions addressed in this study are the extent to which the Gjelsvikfjella rocks are a product of regional rejuvenation of a Mesoproterozoic crust, or whether they result from Pan-African accretion of post-Mesoproterozoic age crust as documented for the Shackleton Range (e.g. Talarico et al., 1999) on the opposite, south-western extension of the Maud Belt (Tessensohn et al., 1999; Bauer et al., 2003a).

Fieldwork was conducted in Gjelsvikfjella in order to establish the deformation history, relative timing of events and to identify important time markers. To resolve the complex tectono-thermal history of the area, new

SHRIMP U–Pb single zircon data were acquired. These new data from Gjelsvikfjella permit an improvement in the geodynamic model for the Maud Belt and thus in palaeogeographic reconstructions prior to the final assembly of Gondwana.

2. Regional geology of the Maud Belt

The Maud Belt consists of Mesoproterozoic to Early Cambrian polyphase deformed upper amphibolite- to granulite-facies metamorphic supracrustal rocks and a variety of pre-, syn- and post-tectonic intrusions. The belt is separated by large glaciers from the Grunehogna Craton to the northwest, which consists of Archaean granite that is overlain by the Mesoproterozoic volcano-sedimentary Ritscherflya Supergroup (Wolmarans and Kent, 1982; Moyes et al., 1995). The oldest rocks recognised throughout the entire belt, from Heimefrontfjella to central Dronning Maud Land, are metavolcanic orthogneisses that yielded U–Pb zircon ages of between 1160 and 1140 Ma (Arndt et al., 1991; Harris et al., 1995; Jacobs et al., 1998; Paulsson and Austrheim, 2003; Board et al., 2005). The oldest intrusive rocks (metatonalitic gneisses) in the Maud Belt preserve similar ages of between 1140 and 1130 Ma (Jacobs et al., 1998; Jackson, 1999; Paulsson and Austrheim, 2003; Board et al., 2005). The overall calc-alkaline signature of these rocks is consistent with the interpretation of them forming part of a larger Mesoproterozoic volcanic arc system (Groenewald et al., 1995; Jacobs et al., 1998; Bauer et al., 2003b), with elevated Nd model ages pointing to derivation from an old, heterogeneous, sublithospheric mantle (Grosch and Bisnath, unpublished data).

Megacrystic orthogneisses occur throughout the Maud Belt. Examples are the so-called Fugitive, Isingen and Sveabreen megacrystic orthogneisses of H.U. Sverdrupfjella (Groenewald et al., 1995), and megacrystic orthogneiss bodies of the Kirwanveggen (Grantham et al., 1995; Harris, 1999). Locally, the alkali feldspar megacrysts display resorption rims suggesting that they are older than the matrix (Frimmel, 2004). This is supported by two distinct SHRIMP U–Pb zircon ages of 1127 ± 12 and 1061 ± 14 Ma obtained on megacrystic orthogneiss from northern Kirwanveggen, which have been interpreted as the age of crystallization and metamorphic matrix recrystallization, respectively (Harris et al., 1995).

SHRIMP U–Pb zircon ages of between 1080 and 1030 Ma that are interpreted to record high-grade metamorphism have been reported from throughout the Maud Belt. These ages were obtained from metamorphic zircon overgrowths in the Heimefrontfjella (Arndt et al.,

granulite-facies assemblage containing orthopyroxene (M_1) are believed to correspond to the older metamorphic zircon overgrowths, dated at between 1080 and 1030 Ma. P – T conditions of 8 to 10 kbar and 850 °C have been estimated for this stage (Groenewald and Hunter, 1991). A second metamorphic stage (M_2) involved the decompression from eclogite-facies conditions (M_{2a}) to conditions transitional between amphibolite and granulite facies ($P = 5$ –8 kbar; $T = 600$ –790 °C; M_{2b} ; Board et al., 2005). Subsequent growth of biotite laths that have identical chemical composition to syn- D_2 biotite laths have been ascribed to K-metasomatism (M_{2c}) that outlasted the main pulse of deformation and was caused by widespread late- to post-orogenic felsic magmatism (Board et al., 2005). Finally, a regional retrogressive metamorphic event (M_3) is evident from chlorite rims on biotite and the formation of epidote. This is ascribed to the break-up of Gondwana and will not be further considered here.

3. Geology of Gjelsvikfjella

The rocks of the Gjelsvikfjella area comprise polydeformed, upper amphibolite-facies gneisses derived from a supracrustal sequence that was intruded by various plutonic and hypabyssal melts. These rocks have been migmatized to various degrees with the main pulse of migmatization being syn-tectonic (relative to D_2), with anatexis outlasting D_2 .

Five mappable units have been recognised in the Gjelsvikfjella area (Fig. 2). The oldest unit observed is a metasupracrustal sequence (referred to here as the Gneiss Complex). It is dominated by biotite–garnet gneiss that occurs as concordant layers alternating with felsic and mafic gneisses of variable composition. The biotite–garnet gneiss contains sillimanite in places with garnet porphyroblasts and syn-kinematic biotite defining S_2 . Two varieties of pre-tectonic mafic bodies are present in the Gjelsvikfjella area. The first variety occurs as mafic lenses and boudins of metabasalt and metagabbro composed of hornblende and plagioclase occurring at different tectonostratigraphic levels in the Gneiss Complex.

The mafic bodies are variably foliated with locally unfoliated garnet amphibolite cores of larger boudins. These cores are in most cases completely surrounded by hornblende and plagioclase. The garnet amphibolite cores consist of garnet, hornblende (mostly as pseudomorphs after clinopyroxene), plagioclase and biotite with minor amounts of quartz, ilmenite, rutile and titanite. The second type is garnet-free amphibolite, which most likely represents re-equilibrated garnet amphibolite

rather than mafic rocks of different composition. The garnet-free amphibolite bodies consist of hornblende, plagioclase and biotite with minor amounts of ilmenite, rutile and titanite. Biotite is typically post-tectonic and occurs as randomly orientated laths.

No evidence of a basement to the above supracrustal sequence has been discovered so far. The oldest plutonic rocks are variably migmatized medium- to coarse-grained granitic and tonalitic augen gneisses, collectively mapped as Migmatite Gneiss. The leucosome domains therein are strongly deformed and thus contrast with the youngest intrusions, which are post-tectonic felsic and mafic dykes (Fig. 3E) and stocks.

The Gjelsvikfjella area is distinguished from western Dronning Maud Land by the abundance of post-tectonic mafic dykes (Fig. 3A). These dykes experienced lower amphibolite- to greenschist-facies metamorphism, are medium- to coarse-grained, melanocratic, hornblende–biotite rocks with no preferred orientation of the constituent minerals. In the northern sector of the study occurs a meta-gabbro body (Stabben gabbro; Fig. 2). This metagabbro is made up of green hornblende, altered brown augite, brown biotite and plagioclase (andesine–oligoclase). A second, light brown biotite generation is also present that overgrew the brown biotite. A coarse-grained variety of the Stabben metagabbro contains a greater percentage of clinopyroxene and olivine. Accessory phases present are apatite, titanite and zircon. Preliminary geochemical analyses indicate that the post-tectonic mafic dykes and the Stabben meta-gabbro have similar major and trace element distribution patterns and also similar isotopic characteristics, suggesting that both types of intrusions were derived from similar mantle sources and may be temporally linked. A coarse-grained undeformed post-tectonic syenite body nearby has been dated at 501 ± 10 Ma (Paulsson and Austrheim, 2003). This syenite is bound to the north by the Stabben metagabbro and to the south by metasupracrustal rocks of the Gneiss Complex (Figs. 2 and 3B).

Primary structures in the rocks of Gjelsvikfjella have been largely obliterated during metamorphism and magmatism. Five deformation events (D_1 – D_5) are recognised in the rocks. Relict structures of the first foliation are preserved in mafic boudins, and rootless isoclinal folds are interpreted to represent F_2 folds. Earlier F_1 folds are difficult to identify, because these folds have been re-orientated by type-3 fold interference patterns (after Ramsay, 1967) during D_2 , implying that there was a continual coaxial refolding of earlier D_1 structures. These F_2 folds have been rotated so that the fold axes now plunge parallel to sub-parallel to the dip direction of the regional pervasive foliation (S_2), i.e. they have a reclined

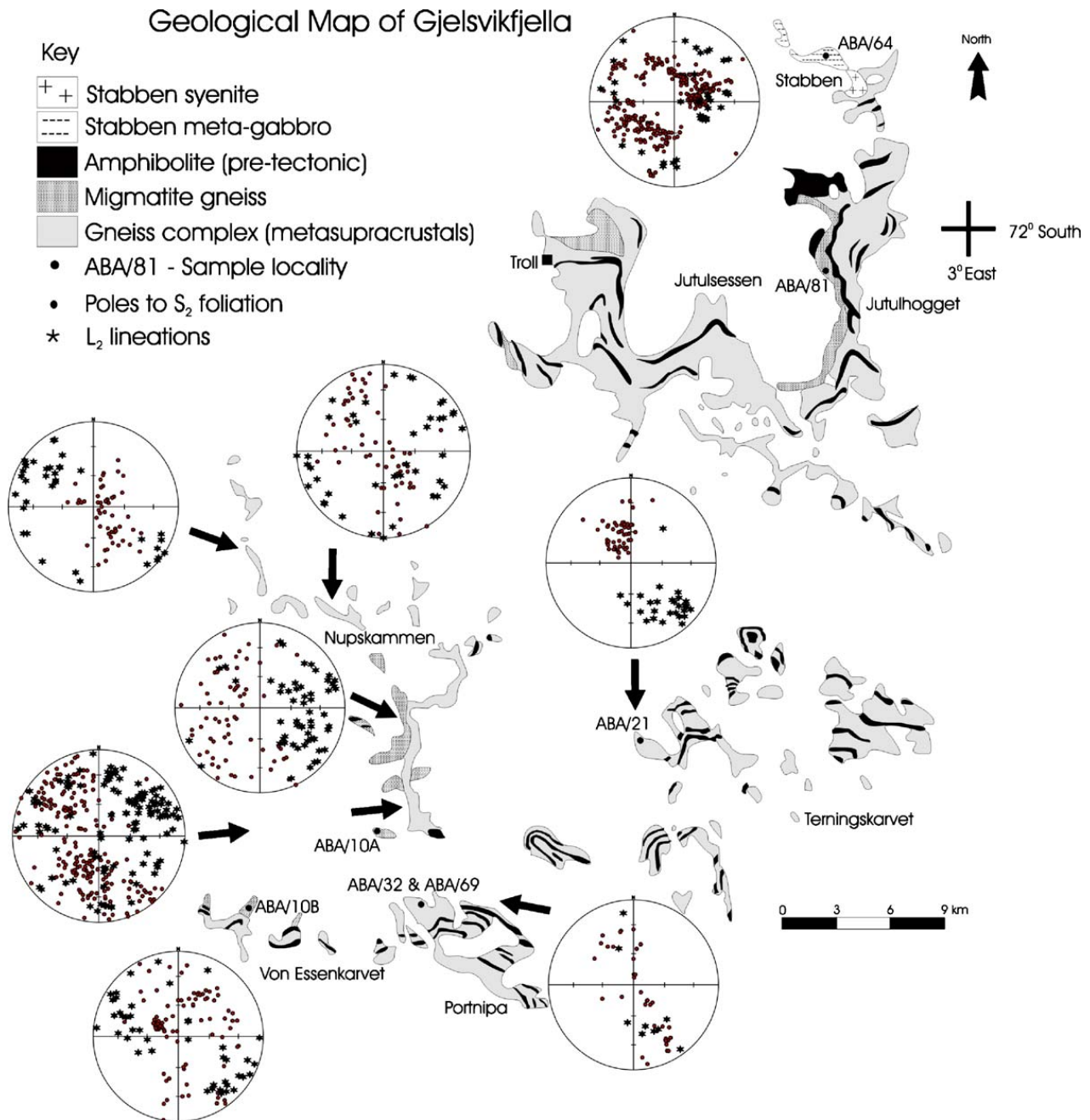


Fig. 2. Geological map of Gjelsvikfjella area modified after Ohta (1999), also shown are sample localities and equal-area stereographic projections of L_2 lineations and poles to S_2 foliation.

attitude (Fig. 3C). The dominant S_2 fabric is parallel to lithological contacts (Fig. 3C and E) and is defined by compositional banding on a centimetre- to metre-scale. The third fabric (S_3) is an axial planar fabric (Fig. 3D), which is preserved as leucosome domains that parallel the F_3 fold axial planes. A fourth deformation event (D_4) is evident as broad open folds or regional scale warping. The youngest deformation (D_5) caused vertical to sub-vertical fractures that are parallel to post-tectonic dolerite intrusions related to Gondwana break-up (Grantham et al., 1995).

4. Samples and methods

Using standard separation techniques (Wilfley table, magnetic separation, heavy liquids and hand picking), zircon grains were separated from seven samples from the Gjelsvikfjella area (Fig. 2). Prior to analysis, photomicrographs and cathodoluminescence (CL) images of sectioned zircon grains were taken in order to characterise the zircon populations, fracture patterns and metamorphic overgrowths. Ion microprobe analyses of zircon populations were carried out using SHRIMP RG at the

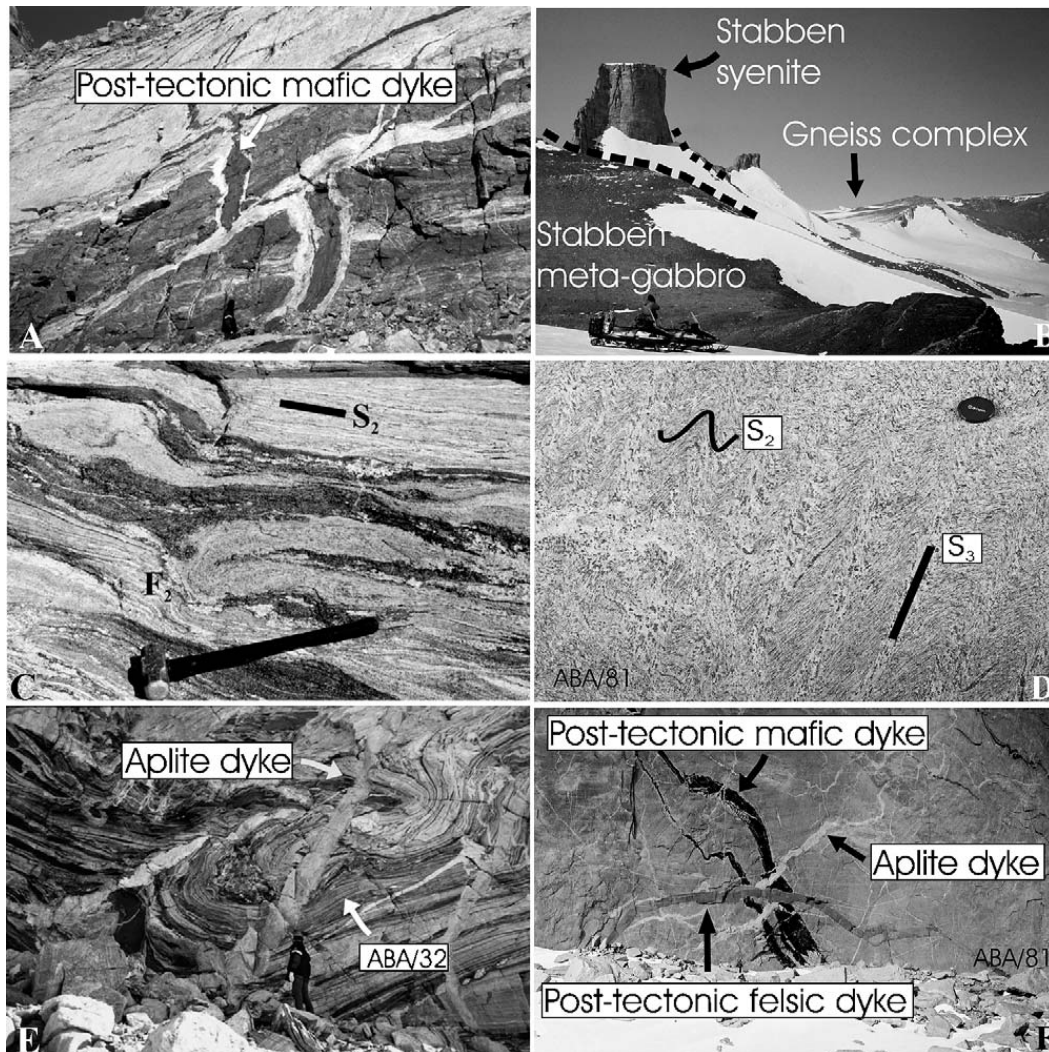


Fig. 3. (A) Post-tectonic dykes that are discordant to the regional foliation; (B) Intrusive relationships (— intrusive contacts) around Stabben; (C) Rootless isoclinal folds showing an early deformation event; (D) Jutulhogget migmatitic gneiss containing leucosomes that are parallel to the axial plane of F_3 folds and sample locality ABA/81; (E) Post-tectonic aplite dykes and locality for sample ABA/32; and (F) Migmatitic gneiss at Jutulhogget also showing post-tectonic dyke relationships and sample locality ABA/81.

Research School of Earth Sciences, Australian National University, Canberra. SHRIMP analytical methods follow those given by Williams (1998) and references therein. U/Pb ratios have been calibrated relative to 1099 Ma Duluth Gabbro reference zircon (see Paces and Miller, 1993) and the data were reduced using the SQUID Excel Macro of Ludwig (2000). For zircon older than 800 Ma common Pb has been corrected using the measured $^{204}\text{Pb}/^{206}\text{Pb}$ ratios, for zircon younger than 800 Ma common Pb was corrected using measured $^{207}\text{Pb}/^{206}\text{Pb}$ and $^{238}\text{U}/^{206}\text{Pb}$ ratios, following Tera and Wasserburg (1972), as described in detail by Compston et al. (1992). Uncertainties in the measured ratios are given at one sigma level and the weighted mean age uncertainties at

95% confidence level (plots and calculation using ISO-PLOT/EX; Ludwig, 1999).

The isotopic data were supplemented by analyses of rare earth element (REE) concentrations on selected zircon grains (Appendix A), using laser ablation inductively coupled mass spectrometry (ICPMS) techniques at the Department of Geological Sciences, University of Cape Town. A Perkin Elmer Elan 6000 instrument, coupled to a Cetac LSX-200 laser ablation module with a 266nm frequency-quadrupled Nd-YAG laser was employed. The NIST 610 and 612 glass standards were used for zircon analyses. Lower detection limits are typically below 20 ppb for the REE, typical precision and accuracy range between 1 to 10 relative percent.

5. Results

5.1. Migmatite Gneiss

Sample ABA/81, a strongly deformed, biotite-rich gneiss was collected from Jutulhogget (72°01'S; 2°50'E; Figs. 2 and 3F). This fine- to medium-grained rock consists of quartz (20 vol.%), plagioclase (25 vol.%), K-feldspar (30 vol.%), biotite (10–15 vol.%) and green hornblende (5–10 vol.%), with trace amounts of zircon, rutile and opaques. Biotite defines the foliation (S_2) and is folded into tight to open folds with the fold axial traces defining a crenulation cleavage (S_3) (Fig. 3D). Simultaneously with the S_3 development partial melting occurred as indicated by the presence of leucosome domains that are parallel to the fold axial traces of the crenulations (Fig. 3D). Sample WBS3 was collected from a syn- S_3 leucosome domain that contains poikilitic hornblende, up to 2 cm in length, within these leucosome domains.

The zircon grains in these two samples are colourless, subhedral to anhedral and 50–300 μm in size. Most of the grains are dipyratidial prismatic, with the $\{100\}$ and $\{101\}$ crystallographic forms dominating, whereas the $\{211\}$ pyramidal form is weakly developed. The grains display variable degrees of rounding with some being ovoid in shape. Cathodoluminescence images (Fig. 5A) show that the zircon cores are characterised by oscillatory zoning (interpreted as magmatic compositional zoning), which is rimmed by three different types of overgrowths. The first overgrowth generation truncates the compositional zonation of the core and displays only weak CL. The second phase of overgrowth is characterised by bright CL, and truncates the first. This bright rim is, in turn, rimmed by an overgrowth that has a weaker CL. The latter appears to have grown parallel to the brightly cathodoluminescent zircon overgrowth implying that the two types of zircon overgrowths might be related to the same event.

Eleven analyses were made of zircon cores from sample ABA/81, and these combined yield an upper intercept age of 1130 ± 19 Ma (Fig. 4A1; MSWD = 0.83; probability of fit = 0.62). Two cores (spot 6.1 and 7.2) that are texturally different from the other cores under CL gave $^{206}\text{Pb}/^{238}\text{U}$ ages of 1207 ± 13 and 1204 ± 13 Ma (ABA 81; Table 2 and Fig. 5A), respectively. Five analyses of magmatic zircon cores from sample WBS3 gave an

indistinguishable $^{207}\text{Pb}/^{206}\text{Pb}$ age of 1133 ± 16 Ma and one core (spot analysis 53.1; Table 2) gave a $^{207}\text{Pb}/^{206}\text{Pb}$ age of 1206 ± 19 Ma (Fig. 4A2; MSWD = 0.54; probability of fit = 0.71). The ca. 1130 Ma ages are interpreted to represent the crystallisation age of the magmatic protolith, whereas the ca. 1200 Ma ages are interpreted to represent inherited zircon cores.

Three analyses (spots 2.1, 3.2 and 13.1) on the first zircon overgrowth with the weak CL in sample ABA/81 (Fig. 4A1 and Table 2) yielded a weighted mean $^{207}\text{Pb}/^{206}\text{Pb}$ age of ca. 1070 Ma. The Th/U ratio of this overgrowth ranges from 0.04 to 0.34. In contrast, spot analyses 7.1 (Fig. 5A), 9.1 and 16.1 (Table 2) gave a weighted mean $^{207}\text{Pb}/^{206}\text{Pb}$ age of ca. 530 Ma for the strongly luminescent (i.e. second generation) rims analysed. Rim analyses for sample WBS3 on both weakly (analysis 61.1; Table 2) and strongly (analysis 16.2; Table 2) cathodoluminescent zircon overgrowths, i.e. overgrowth phases two and three, yielded indistinguishable $^{206}\text{Pb}/^{238}\text{U}$ ages of 524 ± 8 and 528 ± 8 Ma and are therefore considered to have formed during the same event. The Th/U ratio of overgrowth phases two and three is variable (0.01–0.86) and overlaps with that of the older overgrowth (Table 2). In samples ABA/81 and WBS3 the older cores are characterised by U contents ranging from 100 to 1569 and 331 to 603 ppm, respectively, and Th/U ratios between 0.14 and 1.81 for sample ABA/81 and 0.14 and 0.69 for sample WBS3. The U content in the first overgrowth for sample ABA/81 is 572 to 924 ppm with a Th/U ratio from 0.04 to 0.35. Ranges in the U contents for the second and third zircon overgrowth stages in both samples are 272–1399 ppm for the high CL overgrowth and 362–3305 ppm for the weak CL overgrowth with both overgrowths having Th/U ratios of less than 0.05. Such low Th/U ratios are typical of metamorphic zircon overgrowths (Williams, 1998). No systematic difference exists in the Th/U ratio between weakly and strongly cathodoluminescent domains.

Chondrite-normalised REE patterns were obtained for zircon grains from both samples ABA/81 and WBS3 by laser ablation ICPMS (Fig. 6A and B). Both the core and rim (bright CL overgrowth) are enriched in heavy REE relative to light REE with positive Ce and negative Eu anomalies. The rims are less enriched in total REE than the cores. The chemical and geochronological data indicate different generations of zircon growth, which is consistent with the textural observations described.

Fig. 4. U–Pb SHRIMP zircon analyses of samples: (A1 and 2) Migmatite Gneiss, Jutulhogget (ABA/81; WBS3); (B) Augen Gneiss, von Essenskarvet (ABA/10A); (C) Mylonitic augen gneiss von Essenskarvet (ABA/10B); (D) Grey Migmatite Gneiss, Terningskarvet (ABA/21); (E) Banded Gneiss, Von Essenskarvet (ABA/32); (F) Stabben metagabbro (ABA/64); (G) Aplite dyke, Von Essenskarvet (ABA/69). A–E and G are Wetherill plots whereas F is a Tera Wasserburg plot.

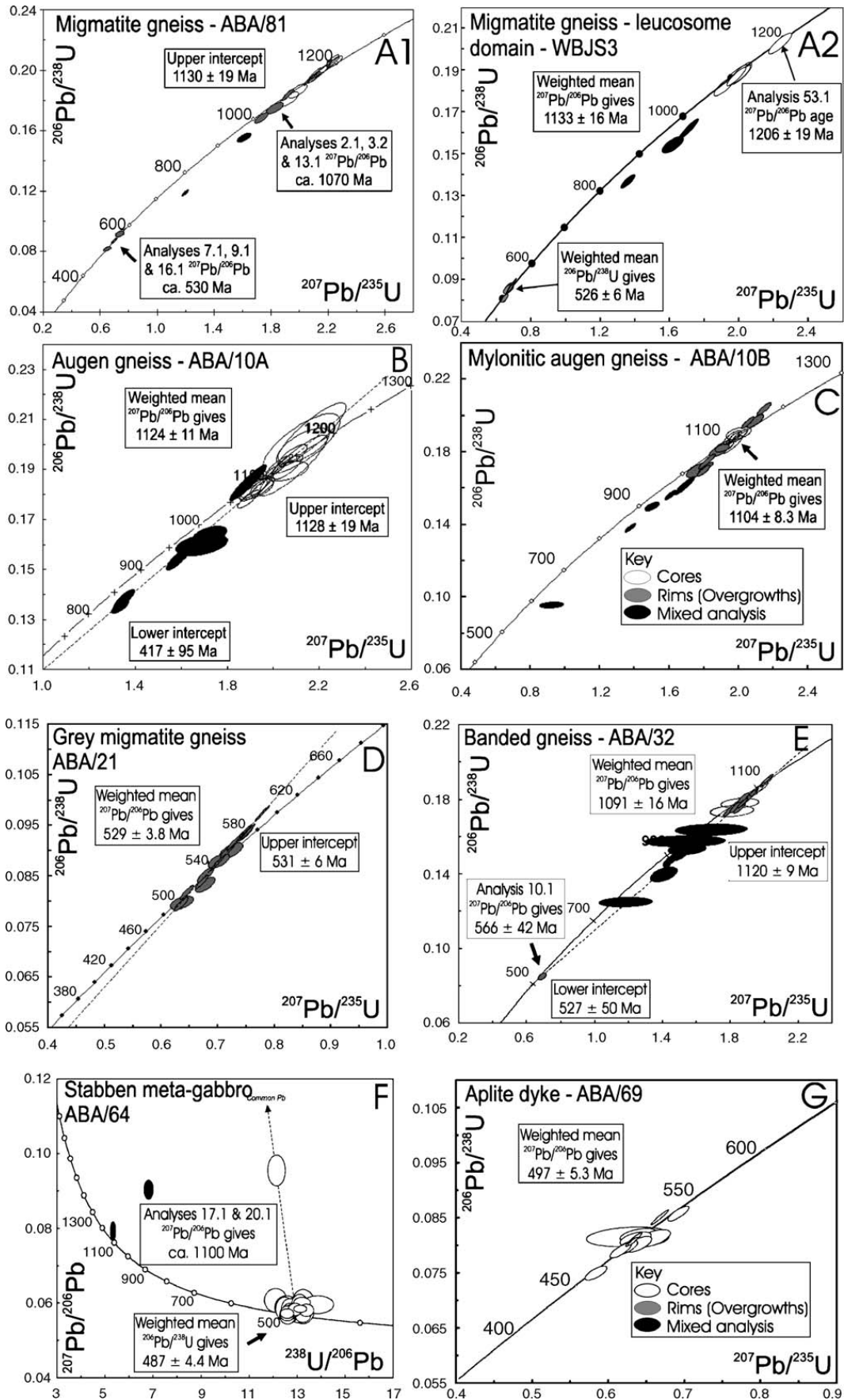


Table 2
SHRIMP U–Pb zircon data for samples ABA/81 and WBJ53

Grain spot ABA/81	U (ppm)	Th (ppm)	$^{232}\text{Th}/^{238}\text{U}$	$^{206}\text{Pb}^*$ (ppm)	f 206%	Radiogenic ratios				Ages (Ma)				Disc (%)		
						$^{207}\text{Pb}^*/^{206}\text{Pb}^*$	$\pm\%$	$^{207}\text{Pb}^*/^{235}\text{U}$	$\pm\%$	$^{206}\text{Pb}^*/^{238}\text{U}$	$\pm\%$	$^{206}\text{Pb}^*/^{238}\text{U}$	$\pm\%$		$^{207}\text{Pb}^*/^{206}\text{Pb}^*$	$\pm\%$
1.1c	571	396	0.72	98.10	0.03	0.08	0.57	2.17	1.50	0.20	1.30	1175	± 14	1165	± 11	-1
2.1r	750	95	0.13	118.00	0.03	0.08	0.56	1.92	1.40	0.18	1.30	1086	± 13	1090	± 11	0
2.2c	111	195	1.81	17.80	0.00	0.08	1.50	1.99	2.20	0.19	1.60	1100	± 16	1132	± 30	3
3.1c	100	100	1.04	15.50	0.00	0.08	1.50	1.93	2.30	0.18	1.80	1071	± 17	1128	± 31	5
3.2r	572	195	0.35	85.80	0.00	0.08	1.50	1.83	2.10	0.17	1.40	1038	± 13	1091	± 30	5
4.1c	701	569	0.84	118.00	0.15	0.08	0.64	2.11	1.30	0.120	1.20	1150	± 12	1151	± 13	0
5.1c	1579	211	0.14	263.00	0.08	0.08	0.37	2.07	1.20	0.19	1.10	1140	± 12	1133	± 7.3	-1
6.1c	493	279	0.58	87.20	0.02	0.08	0.83	2.25	1.40	0.21	1.20	1207	± 13	1182	± 16	-2
7.1r	855	10	0.01	64.00	0.00	0.06	0.76	0.70	1.70	0.09	1.50	539	± 7.6	538	± 17	0
7.2c	1072	1463	1.41	189.00	0.04	0.08	0.43	2.24	1.30	0.21	1.20	1204	± 13	1174	± 8.5	-3
8.1rc	165	70	0.44	23.90	0.07	0.07	1.10	1.73	1.70	0.17	1.40	1003	± 13	1059	± 22	5
9.1r	597	5	0.01	47.10	0.57	0.06	2.30	0.74	2.60	0.09	1.30	564	± 6.7	550	± 50	-2
10.1c	508	417	0.85	90.20	0.00	0.08	0.53	2.23	1.30	2.21	1.20	1211	± 13	1154	± 10	-5
11.1c	1569	212	0.14	267.00	0.01	0.08	0.45	2.11	1.40	0.20	1.30	1164	± 14	1129	± 9.0	-3
12.1rc	1805	330	0.19	184.00	0.25	0.07	0.51	1.20	1.20	0.12	1.10	722	± 7.8	1020	± 10	29
13.1r	924	37	0.04	123.00	0.08	0.08	1.30	1.61	1.80	0.16	1.30	931	± 11	1075	± 26	13
14.1c	1499	1057	0.73	252.00	0.31	0.08	0.64	2.10	1.40	0.20	1.20	1149	± 13	1147	± 13	0
15.1c	807	305	0.39	139.00	0.16	0.08	0.71	2.16	1.50	0.20	1.30	1173	± 14	1157	± 14	-1
16.1r	644	538	0.86	45.50	0.67	0.06	1.90	0.65	2.20	0.08	1.20	506	± 5.7	519	± 42	2
WBJ53																
4.1r	272	8	0.03	21.00	0.72	0.0571	0.0013	0.664	0.020	0.0844	0.0015	522	± 9	496	± 51	-5
9.1r	537	20	0.04	39.00	0.13	0.0582	0.008	0.642	0.014	0.800	0.0013	496	± 8	539	± 29	8
16.1c	476	292	0.61	94.00	0.19	0.0766	0.0008	1.920	0.041	0.1819	0.0031	1077	± 17	1110	± 22	3
16.2r	1392	35	0.03	108.00	0.09	0.0579	0.0004	0.676	0.012	0.0847	0.0013	524	± 8	527	± 14	1
28.1rc	456	110	0.24	71.00	0.69	0.0763	0.0013	1.619	0.040	0.1538	0.0026	922	± 14	1104	± 34	16
41.1r	1810	69	0.04	140.00	0.04	0.0578	0.0004	0.672	0.012	0.0844	0.0013	522	± 8	521	± 15	0
43.1c	548	367	0.67	115.00	0.32	0.0775	0.0008	2.018	0.040	0.1888	0.0031	1115	± 17	1134	± 19	2
43.2r	362	3	0.01	28.00	0.17	0.0567	0.0009	0.665	0.017	0.0850	0.0015	526	± 9	481	± 37	-9
53.1c	423	272	0.64	94.00	0.08	0.804	0.0008	2.244	0.045	0.2025	0.0033	1189	± 18	1206	± 19	1
53.2r	1516	50	0.03	117.00	0.07	0.0578	0.0003	0.670	0.011	0.0841	0.0013	520	± 8	521	± 12	0
56.1r	3303	153	0.05	266.00	0.32	0.0575	0.0002	0.694	0.011	0.0876	0.0013	541	± 8	510	± 9	-6
58.1c	331	143	0.43	65.00	0.19	0.0781	0.0006	2.018	0.040	0.1875	0.0032	1108	± 17	1149	± 16	4
58.2rc	746	106	0.14	117.00	0.11	0.0770	0.003296	1.714	0.038	0.1615	0.0032	965	± 18	1121	± 15	14
59.1c	351	143	0.41	69.00	0.35	0.0774	0.11	2.003	0.045	0.1876	0.0032	1109	± 17	1132	± 26	2
61.1r	1526	80	0.05	120.00	0.04	0.0575	0.0010	0.676	0.012	0.0853	0.0013	528	± 8	510	± 14	-3
65.1c	603	416	0.69	125.00	0.08	0.0773	0.0006	1.989	0.037	0.1866	0.0030	1103	± 16	1130	± 15	2
65.2rc	399	103	0.26	240.00	0.22	0.0724	0.0007	1.359	0.027	0.1361	0.0022	823	± 12	997	± 20	17

Errors are 1-sigma; f 206% is the proportion of common ^{206}Pb , Pb^* is the radiogenic proportion. Error in standard calibration was 0.35% (not included in above errors but required when comparing data from different mounts). (l) Common Pb corrected using measured ^{204}Pb . For disc (%), 0% denotes a concordant analysis. c: core analysis; rc: mixed ages (rim + core); r: metamorphic overgrowth (rim analysis).

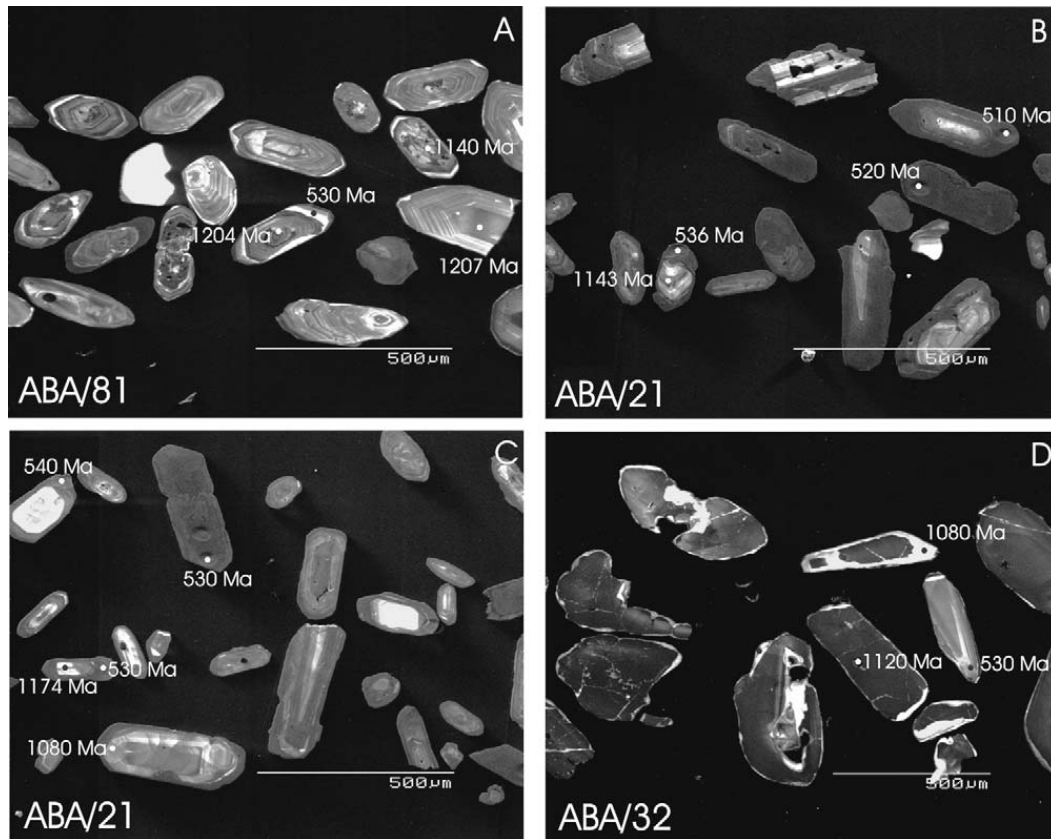


Fig. 5. Cathodoluminescence images of zircon grains. (A) Migmatite Gneiss, Jutulhogget (ABA/81); (B and C) Grey Migmatite Gneiss, Terningskarvet (ABA/21); (D) Banded Gneiss, Von Essenskarvet (ABA/32). Note: the ~530 Ma age presented for sample ABA/81 is a $^{207}\text{Pb}/^{206}\text{Pb}$ and all other ages are $^{206}\text{Pb}/^{238}\text{U}$; for sample ABA/21 all ages are $^{207}\text{Pb}/^{206}\text{Pb}$ ages and for sample ABA/32 the ~530 Ma age presented is a $^{206}\text{Pb}/^{238}\text{U}$ and all other ages are $^{207}\text{Pb}/^{206}\text{Pb}$ ages.

The lower Th/U ratios of the first overgrowth and the lower REE content of the second and third overgrowths indicate that they crystallised during metamorphism (Williams and Claesson, 1987). Consequently, the ca. 1070 and 530 Ma ages most likely represent two metamorphic events.

5.2. Augen Gneiss, Von Essenskarvet

With the aim of determining the emplacement age of the original porphyritic granite and its subsequent metamorphic history, sample ABA/10A was collected from a thick, massive, coarse-grained augen gneiss layer in central Von Essenskarvet ($72^{\circ}12'S$; $2^{\circ}20'E$; Fig. 2). The sample consists of plagioclase, quartz and K-feldspar in approximately equal proportions. The feldspars are generally medium- to coarse-grained with megacrystic plagioclase ranging in size from 1 to 10 cm. Plagioclase (labradorite–bytownite) shows, in places, weak saussurisation and also contains rounded blebs of quartz and elongated quartz inclusions displaying a myrmekitic texture. Two generations of biotite are present. The first generation defines the regional pervasive S_2 fabric, whereas

the second shows no preferred orientation and cuts across S_2 . It is interpreted as post-kinematic and could be related to K-metasomatism that accompanied the nearby post-tectonic Stabben syenite intrusion. Minor amounts of green hornblende and garnet are present with accessory apatite, allanite, zircon and titanite.

Zircon grains in the rock are clear to yellowish-brown and are 20–250 μm in length. Subhedral, elongated grains that are dominated by the $\{100\}$ prismatic and $\{101\}$ pyramidal forms, are common and display rounded terminations. Most zircon grains contain dark inclusions of less than 10 μm in diameter that were carefully avoided during analysis. The zircon grains display well-developed oscillatory magmatic growth zonation in CL images with some grains showing strongly resorbed textures. Cathodoluminescence imaging also revealed a weaker luminescent rim that truncates the zoned cores. These rims do not exceed 10 μm in width and are too small to be analysed.

A total of 16 zircon core analyses (Table 3) yielded a combined weighted mean $^{207}\text{Pb}/^{206}\text{Pb}$ age of 1124.4 ± 11 Ma (MSWD = 0.44; probability of fit = 0.96; Fig. 4B). The five least discordant (<5% discordance) zircon

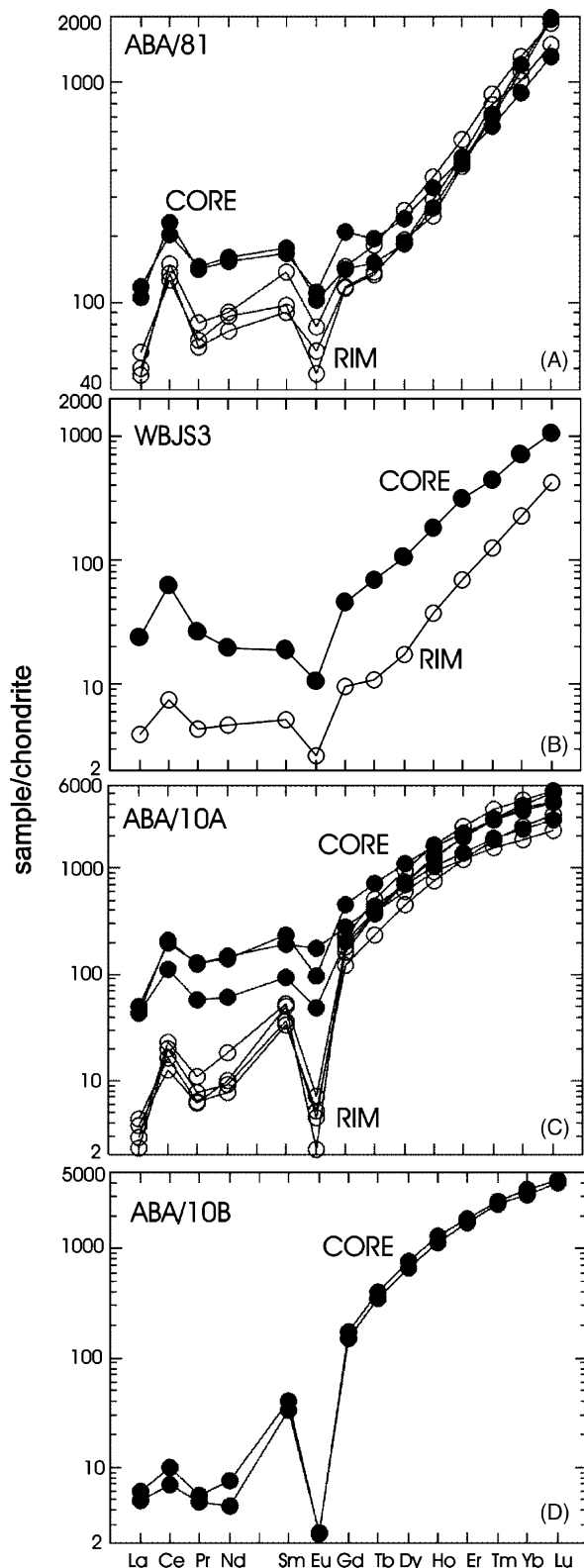


Fig. 6. Chondrite-normalised REE patterns for the cores and rims of selected zircon grains from the following samples: (A and B) Migmatite Gneiss, Jutulhogget (ABA/81 and WBJ3); (C) Augen Gneiss, Von Essenskarvet (ABA/10A); (D) Mylonitic Augen Gneiss, Von Essenskarvet (ABA/10B). Normalisation values are from Sun and McDonough (1989).

analyses gave an upper intercept age of 1128 ± 19 Ma and a lower intercept $^{207}\text{Pb}/^{206}\text{Pb}$ age of 471 ± 95 Ma (Fig. 4B). The upper intercept age and the $^{207}\text{Pb}/^{206}\text{Pb}$ core ages are within error and are interpreted to reflect the crystallization age of the granite protolith, whereas the lower intercept age of 471 ± 95 Ma is interpreted to represent partial Pb loss during Pan-African overprint. Both cores and rims are enriched in heavy REE relative to light REE with positive Ce and negative Eu anomalies (Fig. 6C). The rims are less enriched in total REE than the cores. Thus, the chemical and geochronological data indicate different stages of zircon growth, which is consistent with the textural observations described.

5.3. Mylonitic Augen Gneiss, Von Essenskarvet

A mylonitic augen gneiss (sample (ABA/10B) from western Von Essenskarvet ($72^\circ 13'S$; $2^\circ 13'E$; Fig. 2) was selected in order to determine the emplacement age of the original porphyritic granite and its subsequent metamorphic history. The chosen sample is well foliated and composed of quartz (30 vol.%), biotite (20 vol.%), microcline (30 vol.%) that displays transformation lamellae (Shelley, 1983) with minor amounts of plagioclase (10 vol.%), hornblende (10 vol.%), and trace amounts of apatite, zircon and garnet. The quartz grains are typically stretched out into ribbon and eye shapes. Biotite defines the regional pervasive S_2 fabric and parallels the stretched quartz grains.

Zircon grains in this rock are clear to yellowish-brown and are 20–300 μm in length. They are subhedral, elongated grains dominated by the $\{100\}$ prismatic and $\{101\}$ pyramidal forms. Rounded terminations and marginal resorption are common. Cathodoluminescence images of the zircon grains show oscillatory growth zonation that is interpreted as magmatic. Many grains have a weakly luminescent rim that truncates the zoned cores. These rims are generally 10–15 μm in width and are too small to be analysed (Table 3).

A total of nine zircon core analyses yielded a combined weighted mean $^{207}\text{Pb}/^{206}\text{Pb}$ age of 1104 ± 8 Ma (MSWD = 0.94; probability of fit = 0.52; Fig. 4C). This age is interpreted as the crystallization age of the porphyritic granite. A series of strongly discordant zircon analyses point towards Pb-loss at approximately 1070 Ma (Fig. 4C and Table 4), which is interpreted as resulting from a metamorphic overprint. Core analyses show enrichment in heavy REE relative to light REE with positive Ce and negative Eu anomalies (Fig. 6D). The REE pattern for this sample is similar to the zircon core REE patterns produced for samples ABA/81, WBJ3 and ABA/10A. By analogy, sample ABA/10B is

Table 3
SHRIMP U–Pb zircon data for sample ABA/10A

Grain spot	U (ppm)	Th (ppm)	$^{232}\text{Th}/^{238}\text{U}$	$^{206}\text{Pb}^*$ (ppm)	f 206%	Radiogenic ratios						Ages (Ma)			Disc (%)	
						$^{207}\text{Pb}^*/^{206}\text{Pb}^*$	±%	$^{207}\text{Pb}^*/^{235}\text{U}$	±%	$^{206}\text{Pb}^*/^{238}\text{U}$	±%	$^{206}\text{Pb}/^{238}\text{U}$	$^{207}\text{Pb}/^{206}\text{Pb}$			
1.1rc	746	90	0.12	99.00	0.19	0.07	1.10	1.59	2.20	0.15	1.90	924	±17	1061	±22	13
1.2rc	352	230	0.67	50.0	1.06	0.08	2.50	1.72	2.90	0.16	1.50	976	±13	1105	±50	12
2.1c	646	55	0.09	106.0	0.03	0.08	2.10	2.09	4.70	0.19	4.20	1129	±43	1174	±41	4
2.2c	123	65	0.54	19.20	0.00	0.08	1.30	1.91	2.00	0.18	1.60	1076	±16	1105	±26	3
3.1c	683	54	0.08	107.0	0.00	0.08	0.87	1.94	1.60	0.18	1.30	1085	±13	1120	±17	3
3.2c	671	93	0.14	111.00	0.00	0.08	0.56	2.04	1.40	0.19	1.30	1131	±14	1121	±11	-1
4.1c	578	58	0.10	101.00	0.00	0.08	2.30	2.16	4.60	0.20	4.00	1198	±44	1117	±45	-7
4.2c	443	27	0.06	75.80	0.00	0.08	2.60	2.13	3.40	0.20	2.30	1172	±25	1135	±51	-3
5.1c	402	95	0.24	65.80	0.00	0.08	0.87	2.02	1.70	0.19	1.50	1125	±15	1114	±17	-1
6.1c	241	52	0.22	41.50	0.07	0.08	3.40	2.12	5.20	0.20	3.90	1177	±42	1117	±69	-5
7.1rc	689	43	0.06	81.70	0.05	0.07	1.20	1.35	2.20	0.14	1.90	833	±15	960	±25	13
7.2c	327	103	0.33	51.10	0.00	0.08	2.40	1.92	2.80	0.18	1.50	1078	±15	1105	±47	2
8.1c	1578	54	0.04	260.00	0.47	0.08	1.20	2.06	2.10	0.19	1.70	1126	±17	1156	±24	3
8.2rc	466	55	0.12	65.30	2.04	0.08	4.00	1.69	4.40	0.16	1.80	955	±16	1112	±80	14
9.1rc	764	56	0.08	121.00	0.00	0.07	0.99	1.89	2.80	0.18	2.60	1091	±26	1051	±20	-4
9.2c	735	109	0.15	116.00	0.68	0.08	1.40	1.92	2.10	0.18	1.60	1082	±16	1103	±28	2
10.1c	527	82	0.16	83.00	0.18	0.08	0.99	1.96	1.70	0.18	1.40	1082	±14	1136	±20	5
11.1c	334	50	0.16	51.00	0.00	0.08	0.87	1.89	1.60	0.18	1.40	1056	±13	1125	±17	6
12.1c	495	29	0.06	80.50	0.00	0.08	2.60	2.06	2.90	0.19	1.40	1118	±14	1170	±52	4
13.1c	491	78	0.16	82.60	0.13	0.08	1.20	2.08	1.90	0.20	1.50	1151	±15	1130	±25	-2
13.2rc	372	49	0.14	43.10	0.07	0.07	1.20	1.34	1.90	0.13	1.40	816	±11	979	±25	17

Errors are 1-sigma; f 206% is the proportion of common ^{206}Pb , Pb^* is the radiogenic proportion. Error in standard calibration was 0.48% (not included in above errors but required when comparing data from different mounts). (1) Common Pb corrected using measured ^{204}Pb . For disc (%), 0% denotes a concordant analysis. c: core analysis; rc: mixed ages (rim + core).

Table 4
SHRIMP U–Pb zircon data for sample ABA/10B

Grain spot	U (ppm)	Th (ppm)	$^{232}\text{Th}/^{238}\text{U}$	$^{206}\text{Pb}^*$ (ppm)	f 206%	Radiogenic ratios						Ages (Ma)				Disc (%)
						$^{207}\text{Pb}^*/^{206}\text{Pb}^*$	$\pm\%$	$^{207}\text{Pb}^*/^{235}\text{U}$	$\pm\%$	$^{206}\text{Pb}^*/^{238}\text{U}$	$\pm\%$	$^{206}\text{Pb}/^{238}\text{U}$	$\pm\%$	$^{207}\text{Pb}/^{206}\text{Pb}$	$\pm\%$	
1.1r	940	27	0.03	139.00	0.13	0.08	0.79	1.811	1.50	0.17	1.20	1019	± 12	1117	± 16	10
2.1r	1381	38	0.03	215.00	0.29	0.08	1.50	1.89	2.00	0.18	1.40	1070	± 13	1092	± 29	2
3.1rc	1569	48	0.03	187.00	0.21	0.07	0.68	1.38	1.40	0.14	1.20	835	± 9.6	994	± 14	19
4.1c	800	65	0.08	129.00	0.00	0.08	0.55	1.97	1.30	0.19	1.10	1108	± 12	1098	± 11	-1
5.1c	493	280	0.59	79.90	0.00	0.08	0.73	2.01	1.40	0.19	1.20	1115	± 12	1126	± 15	1
6.1c	200	136	0.70	33.90	0.00	0.08	0.99	2.10	1.60	0.20	1.20	1159	± 13	1127	± 20	-3
7.1rc	3156	247	0.08	425.00	0.37	0.07	0.72	1.61	1.30	0.16	1.10	936	± 9.9	1058	± 14	13
8.1c	476	86	0.19	78.40	0.81	0.08	2.00	2.00	2.40	0.19	1.20	1123	± 12	1103	± 41	-2
9.1rc	1046	44	0.04	135.00	0.10	0.07	1.30	1.50	1.70	0.15	1.10	901	± 9.4	1005	± 27	12
10.1r	353	150	0.44	51.50	0.00	0.08	0.74	1.80	1.40	0.17	1.20	1011	± 11	1119	± 15	11
11.1c	610	74	0.13	98.50	0.09	0.08	1.20	1.97	1.80	0.19	1.40	1109	± 14	1094	± 23	-1
12.1r	352	98	0.29	55.10	0.00	0.08	0.95	1.90	1.90	0.18	1.60	1078	± 16	1089	± 19	1
12.2rc	1889	110	0.06	156.00	0.61	0.07	4.70	0.93	4.80	0.10	1.10	590	± 6.3	928	± 96	57
13.1r	2061	82	0.04	327.00	0.41	0.08	0.96	1.96	2.00	0.18	1.70	1089	± 18	1132	± 19	4
14.1r	740	77	0.11	117.00	0.18	0.08	1.40	1.92	1.80	0.18	1.10	1083	± 11	1096	± 27	1
15.2rc	1003	107	0.11	139.00	0.27	0.08	0.89	1.69	2.20	0.16	2.00	964	± 18	1095	± 18	14
16.1c	4691	63	0.01	823.00	0.29	0.08	0.63	2.15	1.30	0.20	1.10	1194	± 12	1108	± 13	-7
17.1r	1423	58	0.04	214.00	0.03	0.08	0.67	1.82	1.70	0.17	1.50	1038	± 15	1082	± 13	4
18.1r	443	69	0.16	65.00	0.44	0.08	1.90	1.77	2.50	0.17	1.60	1012	± 15	1078	± 38	7
19.1c	7560	127	0.02	1280	0.06	0.08	0.53	2.06	1.20	0.20	1.10	1155	± 12	1093	± 11	-5

Errors are 1-sigma; f 206% is the proportion of common ^{206}Pb , Pb^* is the radiogenic proportion. Error in standard calibration was 0.36% (not included in above errors but required when comparing data from different mounts). (1) Common Pb corrected using measured ^{204}Pb . For disc (%), 0% denotes a concordant analysis. c: core analysis; rc: mixed ages (rim + core); r: metamorphic overgrowth (rim analysis).

interpreted to be of magmatic origin. The rims were too small to be analysed.

5.4. Grey Migmatite Gneiss, Terningskarvet (ABA/21)

A grey migmatite gneiss (Sample ABA/21, 72°10'S; 2°38'E; Fig. 2) was sampled in order to determine the emplacement age of the granite protolith and its subsequent metamorphic history. The chosen sample has a gneissose texture and is composed of quartz (30 vol.%), biotite (20 vol.%) and microcline (45 vol.%) that displays transformation lamellae, with trace amounts of apatite and zircon. Field relationships indicate at least two stages of deformation. F₁ folds have been completely obliterated. Preserved in these rocks are rootless isoclinal folds (F₂) that produced the regional dominant fabric (S₂). This was followed by the re-orientation of F₂ folds so that the fold axes now plunge parallel to the dip of the regional pervasive fabric (S₂), which is defined by the alignment of biotite grains.

This rock contains colourless to yellow and brown, elongated zircon with a grain size ranging from 20 to 300 μm. The grains are subhedral to euhedral and dominated by the {100} prismatic and {101} pyramidal forms. They display rounded terminations, in places leading to an ovoid morphology. Cathodoluminescence images (Fig. 5B and C) of the zircon grains show cores that are highly luminescent with well-developed, presumably magmatic oscillatory growth zonation and resorption textures. The grains have a weaker luminescent rim that truncates the oscillatory growth zonation. The cores have U concentrations ranging from 139 ppm to 495 ppm and Th/U ratios between 0.21 and 0.71. In contrast, the rims are enriched in U (2578–8059 ppm) and thus yield lower Th/U ratios (0.01–0.09; Table 5), which is typical of metamorphic zircon overgrowths (Williams, 1998).

Seventeen analyses were made of zircon rims from sample ABA/21, and these yielded a weighted mean ²⁰⁷Pb/²⁰⁶Pb age of 529 ± 4 Ma (MSWD = 1.08; probability of fit = 0.37) with the most concordant analysis (spot 3.1) giving a ²⁰⁷Pb/²⁰⁶Pb age of 505 ± 10 Ma (Fig. 4D). These ages are interpreted as dating a metamorphic overgrowth. Two core analyses (spot 4.2 and 8.2; Fig. 5B and C) gave a ²⁰⁷Pb/²⁰⁶Pb age of 1143 ± 41 and 1174 ± 45 Ma, respectively. The younger age is interpreted to represent the crystallisation age of the magmatic protolith whereas the older age is interpreted to represent a mixed age. Two strongly luminescent spots were analysed (spot 1.1 and 9.1; Table 5 and Fig. 5C) and yielded a ²⁰⁷Pb/²⁰⁶Pb age of 1048 ± 18

and 1080 ± 13 Ma, respectively, which is within error of ages obtained for other samples (see above) and is interpreted to represent an earlier metamorphic event. However, their Th/U ratio (0.26) is relatively high compared to typical metamorphic overgrowths.

5.5. Banded Gneiss, Von Essenskarvet

A banded gneiss sample (ABA/32) was collected from the vicinity of Portnipa in western Von Essenskarvet, (72°14'S; 2°22'E; Fig. 2) in order to test the inferred sedimentary origin of the rock, to place constraints on the age of the source rocks, and also to define the maximum age of the metasedimentary sequence. The rock is characterised by compositional banding on the centimetre- to metre-scale (Fig. 3E). This is due to the alignment of mafic and felsic metamorphic minerals. The banded gneiss unit contains alternating bands of hornblende-rich, biotite-garnet-rich and felsic bands. The biotite-garnet-rich unit is essentially composed of biotite (40 vol.%), garnet (20 vol.%), plagioclase (20 vol.%), quartz (10 vol.%) and accessory zircon, apatite and in some places sillimanite. The hornblende-rich unit contains bands that display a nematoblastic texture and are made up of hornblende (30 vol.%), plagioclase (25 vol.%), quartz (15 vol.%), diopside (10 vol.%) and biotite (10 vol.%) with accessory zircon, titanite and apatite. The biotite occurs along the margins of the clinopyroxene grains. Locally, clinopyroxene is totally replaced by hornblende. Quartz is stretched into ribbon shapes. Rounded blebs of quartz are present in plagioclase grains displaying a myrmekitic texture.

The zircon grains are generally anhedral, 20–250 μm in length and dark brown in colour. Cathodoluminescence imaging revealed that the majority of the grains are homogeneous and contain weaker luminescent cores with presumably magmatic compositional zonation (Fig. 5D). Some zircon cores contain dark inclusions of up to 10 μm in diameter that were avoided during analyses. The cores are rimmed by brightly luminescent margins. A relatively large proportion of the zircon grains are fractured and have been infilled with brightly luminescent zircon (Fig. 5D). The morphology of these margins implies that they represent a metamorphic overgrowth. Five concordant analyses of bright luminescent zircon rims yielded a weighted mean ²⁰⁷Pb/²⁰⁶Pb age of 1091 ± 16 Ma (MSWD = 1.9; probability of fit = 0.079; Fig. 4E). These rims have relatively high Th/U ratios ranging from 0.31 to 0.47 (Table 6). The least discordant analysis (spot 8.1; Table 6 and Fig. 5D) gave a ²⁰⁷Pb/²⁰⁶Pb age of 1120 ± 9 Ma that is identical to the calculated upper intercept age of 1120 ± 12 Ma

Table 5
SHRIMP U–Pb zircon data for sample ABA/21

Grain spot	U (ppm)	Th (ppm)	$^{232}\text{Th}/^{238}\text{U}$	$^{206}\text{Pb}^*$ (ppm)	f 206%	Radiogenic ratios						Ages (Ma)		Disc (%)		
						$^{207}\text{Pb}^*/^{206}\text{Pb}^*$	$\pm\%$	$^{207}\text{Pb}^*/^{235}\text{U}$	$\pm\%$	$^{206}\text{Pb}^*/^{238}\text{U}$	$\pm\%$	$^{206}\text{Pb}/^{238}\text{U}$	$^{207}\text{Pb}/^{206}\text{Pb}$			
1.1r	420	116	0.28	60.60	0.17	0.07	0.89	1.72	1.90	0.17	1.70	999	± 16	1048	± 18	5
1.2r	2958	33	0.01	213.00	0.77	0.06	1.30	0.68	1.70	0.08	1.20	515	± 5.8	575	± 28	10
2.1r	7916	100	0.01	623.00	0.01	0.06	0.31	0.73	1.10	0.09	1.00	565	± 5.6	517	± 6.9	–9
3.1r	3368	30	0.01	236.00	0.01	0.06	0.48	0.65	1.20	0.08	1.10	506	± 5.4	505	± 10	0
4.1r	4244	108	0.03	290.00	0.28	0.06	0.56	0.64	1.20	0.08	1.10	492	± 5.2	536	± 12	8
4.2c	342	71	0.21	46.10	1.11	0.08	2.10	1.67	2.40	0.16	1.10	931	± 9.9	1143	± 41	19
5.1r	3735	316	0.09	263.00	2.77	0.06	1.70	0.64	2.10	0.08	1.10	494	± 5.2	534	± 38	8
5.2r	11249	69	0.01	845.00	0.01	0.06	0.24	0.70	1.10	0.09	1.10	540	± 5.8	530	± 5.3	–2
6.1r	6782	96	0.01	488.00	0.10	0.06	0.38	0.67	1.10	0.08	1.00	519	± 5.2	539	± 8.2	4
6.2r	2578	18	0.01	196.00	0.82	0.06	1.30	0.70	1.70	0.09	1.10	543	± 5.5	527	± 29	–3
7.1r	8056	36	0.00	649.00	0.01	0.06	0.25	0.75	1.10	0.09	1.00	578	± 5.8	541	± 5.4	–7
8.1r	2216	131	0.06	163.0	0.41	0.06	0.86	0.68	1.40	0.09	1.10	527	± 5.8	524	± 19	–1
8.2rc	139	96	0.71	18.60	0.96	0.08	2.30	1.69	2.70	0.15	1.30	928	± 12	1174	± 45	21
9.1r	495	126	0.26	78.10	0.07	0.08	0.63	1.91	1.40	0.18	1.30	1086	± 13	1080	± 13	–1
10.1r	7787	167	0.02	625.00	0.08	0.06	0.48	0.75	1.10	0.09	1.00	575	± 5.7	538	± 11	–7
10.2r	15815	237	0.02	1,320	–	0.06	0.20	0.78	0.10	0.10	1.00	599	± 5.9	529	± 4.4	–13
11.1r	2206	76	0.04	172.00	0.71	0.06	1.40	0.72	1.80	0.09	1.10	556	± 6.0	542	± 30	–3
12.1r	4912	66	0.01	388.00	0.00	0.06	0.30	0.73	1.10	0.09	1.00	566	± 5.7	523	± 6.7	–8
13.1r	4604	17	0.00	367.00	0.01	0.06	0.32	0.74	1.10	0.09	1.00	572	± 5.7	524	± 7.1	–9
14.1r	7768	232	0.03	626.00	0.01	0.06	0.23	0.75	1.10	0.09	1.00	578	± 5.7	524	± 5.0	–10
15.1r	4253	73	0.02	330	0.19	0.06	0.52	0.72	1.20	0.09	1.00	556	± 5.6	521	± 11	–7

Errors are 1-sigma; f 206% is the proportion of common ^{206}Pb , Pb^* is the radiogenic proportion. Error in standard calibration was 0.48% (not included in above errors but required when comparing data from different mounts). (1) Common Pb corrected using measured ^{204}Pb . For disc (%), 0% denotes a concordant analysis. c: core analysis; rc: mixed ages (rim + core); r: metamorphic overgrowth (rim analysis).

Table 6
SHRIMP U–Pb zircon data for sample ABA/32

Grain spot	U (ppm)	Th (ppm)	$^{232}\text{Th}/^{238}\text{U}$	$^{206}\text{Pb}^*$ (ppm)	f 206%	Radiogenic ratios						Ages (Ma)			Disc (%)	
						$^{207}\text{Pb}^*/^{206}\text{Pb}^*$	$\pm\%$	$^{207}\text{Pb}^*/^{235}\text{U}$	$\pm\%$	$^{206}\text{Pb}^*/^{238}\text{U}$	$\pm\%$	$^{206}\text{Pb}/^{238}\text{U}$	$^{207}\text{Pb}/^{206}\text{Pb}$			
1.1rc	324	79	0.25	46.30	5.32	0.07	10.00	1.53	10.00	0.16	1.20	944	± 11	945	± 200	0
1.2rc	312	83	0.27	42.00	2.33	0.07	4.50	1.55	4.60	0.15	1.20	919	± 10	1018	± 91	10
1.3c	1277	522	0.42	199.00	0.02	0.08	0.50	1.92	1.50	0.18	1.40	1076	± 14	1110	± 10	3
2.1c	908	368	0.42	146.00	0.07	0.08	0.64	1.99	1.20	0.19	1.00	1104	± 10	1125	± 13	2
2.2r	1076	433	0.42	161.00	0.03	0.07	0.56	1.80	1.60	0.17	1.40	1037	± 14	1066	± 11	3
3.1r	988	397	0.41	154.00	2.00	0.08	3.80	1.86	4.00	0.18	1.00	1056	± 10	1087	± 77	3
4.1r	571	170	0.31	86.90	1.97	0.08	4.60	1.81	4.70	0.17	1.10	1033	± 11	1082	± 91	5
5.1c	1762	1194	0.70	288.00	0.01	0.08	0.36	2.02	1.20	0.19	1.10	1123	± 12	1116	± 7.1	–1
6.1c	1228	539	0.45	185.00	0.07	0.08	0.56	1.86	1.20	0.18	1.00	1042	± 9.9	1116	± 11	7
6.3rc	242	74	0.31	27.10	3.98	0.07	8.60	1.19	8.70	0.13	1.30	759	± 9.2	893	± 180	15
7.1c	612	195	0.33	97.30	0.06	0.08	0.68	1.95	1.30	0.18	1.00	1093	± 11	1113	± 14	2
8.1c	965	393	0.42	157.00	0.00	0.08	0.45	2.01	1.10	0.19	1.00	1119	± 10	1120	± 9.0	0
9.1rc	268	79	0.31	34.60	0.11	0.07	1.30	1.51	1.80	0.15	1.30	902	± 11	1006	± 25	10
9.2c	937	372	0.41	143.00	0.00	0.08	0.46	1.87	1.10	0.18	1.00	1056	± 9.9	1102	± 9.2	4
10.1r	152	16	0.11	11.20	0.00	0.06	1.90	0.69	2.30	0.09	1.30	527	± 6.5	566	± 42	7
12.1r	1008	454	0.47	152.00	0.22	0.08	0.74	1.83	1.30	0.18	1.00	1044	± 9.8	1085	± 15	4
13.1rc	514	121	0.24	74.20	2.49	0.07	8.00	1.69	8.10	0.16	1.20	978	± 11	1064	± 160	8
14.1rc	754	296	0.41	102.00	0.15	0.07	0.74	1.58	1.30	0.16	1.10	938	± 9.3	1012	± 15	7
15.1rc	210	79	0.39	26.60	1.900	0.07	1.10	1.45	1.90	0.15	1.60	888	± 13	964	± 23	8
15.2rc	564	92	0.17	68.70	1.14	0.07	3.10	1.41	3.60	0.14	1.80	845	± 15	1011	± 62	16
16.2r	492	191	0.40	76.40	6.40	0.08	0.59	1.88	1.20	0.18	1.00	1071	± 10	1079	± 12	1

Errors are 1-sigma; f 206% is the proportion of common ^{206}Pb , Pb^* is the radiogenic proportion. Error in standard calibration was 0.28% (not included in above errors but required when comparing data from different mounts). (1) Common Pb corrected using measured ^{204}Pb . For disc (%), 0% denotes a concordant analysis. c: core analysis; rc: mixed ages (rim + core); r: metamorphic overgrowth (rim analysis).

(MSWD=0.98; probability of fit=0.48). As this is the oldest age obtained for this sample, it is interpreted to be the maximum age of sedimentation. The ca. 1090 Ma age calculated is interpreted to be dating metamorphic overgrowth on the basis of textural and chemical evidence even though the Th/U ratio is high when compared to typical metamorphic overgrowths. A calculated lower intercept age of 527 ± 50 Ma is interpreted to reflect a second metamorphic event, which finds support from a $^{207}\text{Pb}/^{206}\text{Pb}$ age of 566 ± 42 Ma on a brightly luminescent spot (spot 10.1; Table 6 and Fig. 4E).

5.6. Stabben Metagabbro

The late- to post-tectonic Stabben metagabbro ($72^{\circ}56'S$; $2^{\circ}47'E$; Figs. 2 and 3B) was sampled in order to determine its emplacement age. The rock is medium- to coarse-grained with no preferred orientation of the constituent minerals. Xenoliths of the host gneiss can be found randomly distributed and locally, the gabbro is cross-cut by pegmatite dykes. The analysed sample (ABA/64) contains saussuritised plagioclase (25 vol.%), green hornblende (30 vol.%), biotite (25 vol.%), altered clinopyroxene (chloritic rims; 10 vol.%), opaques (5 vol.%) and trace amounts of apatite, titanite and zircon.

The zircon grains are clear and up to $250 \mu\text{m}$ in length. Their grain boundaries are irregular, and appear to have irregular zoning that could be a result of rapid grain growth. Their U concentrations are low (41–829 ppm) with Th/U ratios ranging between 0.80 and 2.92.

Twenty-three analyses were made of zircon cores and 21 of these yielded a weighted mean $^{207}\text{Pb}/^{206}\text{Pb}$ age of 487 ± 4 Ma (MSWD=0.62; probability of fit=0.84; Fig. 4F). This is interpreted to represent the magmatic crystallization age of the gabbro body. The remaining two spot analyses (17.1 and 20.1; Table 7) gave much higher ages of 1165 ± 41 and 1090 ± 81 Ma. Based on the post-tectonic intrusive field relationships, these ages cannot date the emplacement or any other process affecting the gabbro, and they are therefore interpreted as inheritance from the host gneiss into which the gabbro intruded.

5.7. Aplite Dyke, Von Essenskarvet

An aplite sample (ABA/69) was collected in western Von Essenskarvet in the vicinity of Portnipa ($72^{\circ}14'S$; $2^{\circ}22'E$; Fig. 2) from a metre-wide, fine- to medium-grained dyke (Fig. 3E). This aplite dyke is undeformed and its age should thus provide a minimum constraint on the timing of deformation in the area. The sample

is equigranular with a grain size of 0.5 to 1.2 mm and composed of microcline (35 vol.%), partly saussuritised plagioclase (25 vol.%), quartz (25 vol.%), and biotite (10 vol.%), with trace amounts of zircon, apatite and muscovite.

Zircon in this rock is colourless to light yellow in colour and between $50 \mu\text{m}$ and $250 \mu\text{m}$ in length. Cathodoluminescence images reveal two zircon populations. The first population is generally smaller, stubby and idiomorphic, of dipyrarnidal prismatic habit with dominance of the $\{100\}$ prism and $\{101\}$ pyramidal forms. This population also shows oscillatory growth zonation. Its U concentration ranges from 358 to 7459 ppm and Th/U ratios are between 0.06 and 1.12. The second population is generally elongate, less euhedral, with very thin rims and $\{100\}$ prism and $\{101\}$ pyramidal forms dominating. This generation has, on average, lower U concentrations (93–848 ppm) with Th/U ratios between 0.67 and 0.12.

The sample yielded a crystallisation age, and thus, by inference, a minimum age for the Pan-African deformation, of 498 ± 5 Ma (MSWD=1.1) on 13 zircon core analyses (Fig. 4G). Analyses on the second population of zircons (spots 2.1, 7.1, 8.1, 14.1, 18.1 and 19.1; Table 8) produced a less dominant discordant age group of between 1100 and 950 Ma (not included in concordia diagram, Fig. 4G) and are interpreted to reflect zircon inheritance from the host rock.

6. Geodynamic model for the Maud Belt

New data acquired in this study, together with recently published data from other parts of the Maud Belt, make it possible to distinguish a series of tectono-thermal events and place relatively precise age constraints on these events (Table 9). Some of these new data are not consistent with previous models for the tectonic evolution along the southern and eastern margins of the Kaapvaal-Grunehogna Craton, particularly during late Mesoproterozoic times. The so far oldest rocks known from Gjelsvikfjella formed within an approximately 1130 Ma volcanic arc, contemporaneous with arc magmatism along the entire length of the Maud Belt. In previous models (e.g. Groenewald et al., 1991; Jacobs et al., 1993) this arc has been linked with an oceanic island arc to the south of the craton, remnants of which are preserved in the Natal sector of the Namaqua-Natal Belt in South Africa. However, available data from that sector (Cornell et al., 1996; Thomas et al., 1999; Johnston et al., 2001) point to arc magmatism having occurred there some 70 myr earlier. Further west, in the Namaqua sector of that belt, arc magmatism commenced even earlier

copy

Table 7
SHRIMP U–Pb zircon data for sample ABA/64

Grain spot	U (ppm)	Th (ppm)	²³² Th/ ²³⁸ U	²⁰⁶ Pb* (ppm)	f 206%	Radiogenic ratios						Ages (Ma)				Disc (%)
						²⁰⁷ Pb*/ ²⁰⁶ Pb*	±%	²⁰⁷ Pb*/ ²³⁵ U	±%	²⁰⁶ Pb*/ ²³⁸ U	±%	²⁰⁶ Pb*/ ²³⁸ U	±%	²⁰⁷ Pb*/ ²⁰⁶ Pb	±%	
1.1c	41	52	1.32	2.91	0.00	0.06	3.50	0.69	4.30	0.08	2.60	511	±13	639	±74	20
2.1c	87	141	1.67	5.87	0.00	0.06	2.90	0.62	3.40	0.08	1.80	487	±8.4	513	±64	5
3.1c	49	63	1.33	3.31	0.00	0.06	3.40	0.65	4.30	0.08	2.60	493	±12	570	±75	14
3.2c	162	314	2.01	11.0	0.00	0.06	2.00	0.63	2.50	0.08	1.50	492	±7.3	498	±44	1
4.1c	156	158	1.04	10.40	0.00	0.06	2.00	0.62	2.50	0.08	1.60	483	±7.2	536	±44	10
5.1c	147	176	1.23	9.90	0.00	0.06	2.10	0.63	2.60	0.08	1.60	486	±7.4	526	±46	8
6.1c	52	40	0.80	3.56	0.00	0.06	3.60	0.65	4.10	0.08	2.00	496	±9.6	555	±79	11
7.1c	255	329	1.33	16.60	0.26	0.06	1.90	0.61	2.60	0.08	1.70	469	±7.9	540	±42	13
8.1c	829	1344	1.68	54.10	0.13	0.06	1.20	0.60	1.90	0.08	1.40	472	±6.6	514	±26	8
9.1c	195	442	2.34	13.00	0.00	0.06	1.80	0.62	2.40	0.08	1.50	480	±7.0	549	±40	13
10.1c	312	883	2.92	21.30	0.00	0.06	1.50	0.63	2.10	0.08	1.40	492	±6.8	508	±32	3
11.1c	194	399	2.12	13.20	0.00	0.06	1.90	0.63	2.40	0.08	1.50	491	±7.2	524	±42	6
11.2c	57	59	1.07	3.66	0.00	0.06	5.20	0.62	5.80	0.08	2.50	468	±11	578	±110	19
12.1c	177	262	1.53	109.0	0.00	0.06	2.60	0.59	4.00	0.07	3.10	448	±13	595	±56	25
13.1c	60	54	0.93	4.24	3.27	0.07	15.00	0.75	15.00	0.08	2.30	493	±11	882	±320	44
13.2c	287	324	1.16	18.60	0.00	0.06	2.00	0.59	2.50	0.08	1.50	469	±6.9	481	±44	3
14.1c	112	229	2.11	7.33	0.47	0.06	4.10	0.59	4.50	0.08	1.80	471	±8.0	457	±91	-3
15.1c	109	174	1.65	7.41	1.00	0.06	2.70	0.62	3.20	0.08	1.70	491	±8.1	486	±59	-1
16.1c	211	300	1.47	13.50	0.00	0.06	1.90	0.60	2.40	0.07	1.50	463	±6.8	539	±41	14
17.1c	549	166	0.31	88.60	0.09	0.08	2.10	2.04	2.50	0.19	1.40	1108	±14	1165	±41	5
18.1c	84	120	1.48	5.65	0.39	0.06	4.50	0.60	4.80	0.08	1.90	485	±8.9	429	±99	-13
19.1c	69	74	1.11	4.50	0.00	0.06	3.40	0.61	4.30	0.08	2.70	475	±12	527	±74	10
20.1c	616	128	0.21	77.60	1.75	0.08	4.00	1.51	4.50	0.14	1.90	868	±15	1090	±81	20

Errors are 1-sigma; f 206% is the proportion of common ²⁰⁶Pb, Pb* is the radiogenic proportion. Error in standard calibration was 0.48% (not included in above errors but required when comparing data from different mounts). Common Pb corrected using measured ²⁰⁴Pb. Common Pb corrected by assuming ²⁰⁶Pb/²³⁸U–²⁰⁷Pb/²³⁵U age-concordance. For disc (%), 0% denotes a concordant analysis. c: core analysis; ic: inherited core.

Table 8
SHRIMP U–Pb zircon data for sample ABA/69

Grain spot	U (ppm)	Th (ppm)	$^{232}\text{Th}/^{238}\text{U}$	$^{206}\text{Pb}^*$ (ppm)	f 206%	Radiogenic ratios						Ages (Ma)				Disc (%)
						$^{207}\text{Pb}^*/^{206}\text{Pb}^*$	$\pm\%$	$^{207}\text{Pb}^*/^{235}\text{U}$	$\pm\%$	$^{206}\text{Pb}^*/^{238}\text{U}$	$\pm\%$	$^{206}\text{Pb}/^{238}\text{U}$	$^{207}\text{Pb}/^{206}\text{Pb}$	$\pm\%$	$\pm\%$	
1.1c	358	97	0.28	24.90	0.10	0.06	1.80	0.66	2.20	0.08	1.30	502	± 6.2	566	± 40	11
2.1ic	1088	113	0.11	157.00	0.42	0.08	1.90	1.75	2.30	0.17	1.40	999	± 13	1092	± 38	9
3.1c	2104	173	0.09	155.00	0.00	0.06	0.77	0.69	1.30	0.09	1.00	530	± 5.3	552	± 17	4
4.1c	7074	2240	0.33	516.00	–	0.06	0.26	0.67	1.10	0.08	1.10	525	± 5.4	492	± 5.8	–7
5.1c	7459	410	0.06	518.00	0.13	0.06	0.35	0.63	1.10	0.08	1.00	501	± 5.0	486	± 7.8	–3
6.1c	815	236	0.30	55.20	0.04	0.06	0.93	0.62	1.50	0.08	1.20	489	± 5.6	482	± 21	–2
7.1ic	720	168	0.24	110.00	0.01	0.08	0.52	1.88	1.20	0.18	1.10	1052	± 11	1124	± 10	6
8.1ic	848	98	0.12	143.00	0.02	0.08	11.00	2.19	11.00	0.20	3.30	1156	± 35	1222	± 210	5
9.1c	729	726	1.03	53.10	3.99	0.06	5.50	0.63	5.70	0.08	1.50	504	± 7.1	443	± 120	–14
10.1c	751	731	1.01	51.60	0.13	0.06	1.30	0.64	1.80	0.08	1.20	496	± 5.6	531	± 28	7
11.1c	574	425	0.76	39.20	0.09	0.06	1.10	0.62	1.60	0.08	1.10	492	± 5.2	493	± 25	0
12.1c	528	181	0.35	69.60	0.06	0.07	0.82	1.50	1.50	0.15	1.20	920	± 11	959	± 17	4
13.1c	1225	999	0.84	78.60	0.19	0.06	1.10	0.58	1.60	0.07	1.20	464	± 5.2	484	± 24	4
14.1ic	121	60	0.51	15.50	0.00	0.07	1.90	1.48	2.40	0.15	1.40	892	± 12	990	± 39	10
15.1c	741	801	1.12	52.60	1.35	0.06	2.30	0.64	2.50	0.08	1.10	505	± 5.3	489	± 51	–3
16.1c	609	537	0.91	42.50	0.62	0.06	3.10	0.65	3.30	0.08	1.10	501	± 5.3	534	± 67	6
17.1c	799	560	0.72	56.00	0.92	0.06	1.80	0.64	2.10	0.08	1.10	502	± 5.3	491	± 40	–2
18.1ic	116	51	0.45	13.30	0.00	0.07	2.60	1.31	3.70	0.13	2.70	803	± 20	971	± 52	17
19.1ic	93	60	0.67	13.90	0.13	0.07	2.50	1.76	2.90	0.17	1.30	1029	± 13	1037	± 51	1

Errors are 1-sigma; f 206% is the proportion of common ^{206}Pb , Pb^* is the radiogenic proportion. Error in standard calibration was 0.48% (not included in above errors but required when comparing data from different mounts). (1) Common Pb corrected using measured ^{204}Pb . For disc (%), 0% denotes a concordant analysis, A103. c: core analysis; ic: inherited core.

copy

Table 9
Summary of the most reliable age data for the Maud Belt, Antarctica

	Central Kirwangeggen Southwest	Northern Kirwanveggen	Sverdrupfjella	Gjelsvikfjella	Festninga/Risemedet	Central Dronning Maud Land Northeast
Rock type/Mineral dated	Jackson (1999)	Harris et al. (1995)	Board et al. (2005)	This study	Jacobs et al. (2003a, 2003b, 2003d)	Jacobs et al. (1998, 2003c)
Stabben Gabbro				483 ± 11 ^a 487.3 ± 4.4		
Granite/Aplite Dykes		475 ± 10	480 ± 13 ^b	497 ± 5	486.9 ± 3.8	
Stabben Syenite				500 ± 8 ^c		
Zircon Overgrowths (Rims)				504 ± 6 ^c		
Lamprophyre Dyke					523 ± 4.8	
Charnokite					521.3 ± 3.4	
Zwiesel Gabbro						527 ± 5
Zircon Overgrowths (Rims)			528 ± 6	529 ± 4	528 ± 10	ca. 530
Syn-tectonic monazite			539 ± 9			
Granite Leucosome					558 ± 5.6	
Zircon Overgrowths (Rims)		585 ± 20	565 ± 11	ca. 570		ca. 570
Granite Dykes	980 ± 13					
Porphyritic Granite Dyke	1011 ± 8					
Zircon Overgrowths (Rims)	1081 ± 4	1061 ± 14	1035 ± 21	ca. 1070	1061 ± 56	ca. 1080
Migmatite Augen Gneiss	1074 ± 11	1103 ± 13		1104 ± 8	1096 ± 8.4	1076 ± 14
Grey Migmatite Gneiss					1115 ± 12	
Augen Gneiss		1127 ± 12		1124 ± 11	1123 ± 21	
Migmatite Augen Gneiss					1137 ± 14	
Granite Gneiss	1134 ± 11	1131 ± 25		1133 ± 16 1163 ± 6 ^c 1130 ± 19		1130 ± 12
Grey Gneiss/Zircon Cores	1143 ± 11	1139 ± 12	1132 ± 16	ca. 1140	1142 ± 21	

All ages in (Ma) derived from SHRIMP U–Pb zircon data, except for:

^a SHRIMP U–Pb titanite age (Jacobs et al., 2003b).

^b Conventional U–Pb zircon age (Board et al., 2005).

^c SIMS U–Pb–Th zircon ages (Paulsson and Austrheim, 2003).

(Frimmel, 2004). Apart from significant differences in the timing of arc magmatism, different kinematic vectors for the accretion of arc material onto the Kaapvaal-Grunehogna Craton speak against a single, continuous volcanic arc stretching all around the craton from the Namaqua-Natal to the Maud Belt.

For the Natal sector, subduction away from the craton has been suggested to explain the postulated oceanic island arc there (Jacobs and Thomas, 1994; Arima et al., 2001) and, by analogy, a similar outboard direction of subduction has also been suggested for the Maud Belt (Bauer et al., 2003b; Basson et al., 2004). Such a model implies a forearc position for the volcano-sedimentary Ritscherflya Supergroup between the Maud Belt and the Grunehogna Craton. The geochemistry of the basin fill points to sediment derivation from an active volcanic arc system (Basson et al., 2004). Magmatic zircon ages of 1131 ± 7 Ma from pyroclastic beds in the lower Ritscherflya Supergroup (Frimmel, 2004) indicate sedimentation to have occurred at the same time as volcanic arc formation. The arc preserved in the Maud Belt is therefore regarded as the main source for the sediments and pyroclastic rocks in the Ritscherflya Basin. The presence of rare older, inherited zircon grains in the various high-grade metamorphic rocks of the Maud Belt, as established in this study for the Gjelsvikfjella and by others for the Heimefrontfjella (Arndt et al., 1991; Jacobs et al., 1996) and the northern Kirwanveggen (Harris, 1999), ranging from 1200 to 2100 Ma, together with Nd model ages as old as Archaen (Grosch and Bisnath, unpublished data), indicate that the Maud arc was not an oceanic island arc but formed adjacent to an Archean craton, presumably the Grunehogna Craton. Consequently, the direction of subduction that led to the formation of the Maud arc, is suggested to have been inboard beneath the Kaapvaal-Grunehogna Craton (Fig. 7A).

U–Pb single zircon ages of 1128 ± 19 and 1104 ± 8 Ma obtained in this study for the Augen Gneiss and Mylonitic Augen Gneiss units in Gjelsvikfjella, respectively, are indistinguishable from an age of 1127 ± 12 Ma obtained for a megacrystic augen gneiss that occurs over a strike length of approximately 300 km along the western Maud Belt and a second generation of megacrystic orthogneiss that has been dated at 1103 ± 13 Ma in the northeastern parts of the Maud Belt (Harris et al., 1995). The older age group around 1127 Ma conforms to the final stages of arc development and the megacrystic granitic protoliths are therefore interpreted as products of arc magmatism.

More ambiguous is the interpretation of the age data clustering around 1100 Ma. Indistinguishable ages have been obtained from similar augen gneiss in the Namaqua

Belt (1109 ± 7 Ma; Raith et al., 2003) and from a granophyre in Coats Land (1106 ± 3 Ma; Gose et al., 1997). This is identical to a precise age of 1105 ± 2 Ma (Hanson et al., 1998, 2004) for tholeiitic sills in eastern Zimbabwe (Umkondo Province) and also to that of 1102 ± 8 Ma obtained for voluminous tholeiite emplacement in the Mid Continental Rift in the southwest Grenville Orogen (Paces and Miller, 1993) as well as in the Warakurna igneous province of west-central Australia (Wingate et al., 2004). For the contemporaneity of these magmatic events over a very large area, their cause has been ascribed to a large-scale, but short-lived mantle thermal anomaly (Hanson et al., 1998). Such a thermal anomaly would have led to decompression melting in the lower crust and upper mantle (Fig. 7B), which, in turn, could have formed the megacrystic granites of that particular age group (Frimmel, 2004). Bimodal magmatism is expected for such decompression melting in a presumably thinning crust. Mafic dykes, now present as pre-tectonic amphibolite bodies, might well be expressions of the same thermal event, but are awaiting precise dating.

The ca. 1070 Ma ages obtained from metamorphic zircon overgrowths in this study record a period of first high-grade metamorphism. Outcrop-scale expressions of this metamorphic event are difficult to recognise due to the intensity of later Pan-African tectono-thermal overprint. Comparable ages for high-grade metamorphism, ranging from 1090 to 1030 Ma, have been reported from most other parts of the Maud Belt (Arndt et al., 1991; Jacobs et al., 1998, 1999, 2003d; Jackson, 1999; Harris, 1999; Paulsson and Austrheim, 2003; Board et al., 2005) and are identical to those reported for comparable high-grade metamorphism in the Namaqua-Natal Belt (Robb et al., 1999; Frimmel, 2004). The contiguity of the Namaqua-Natal and the Maud Belt was therefore established only at the end of the Mesoproterozoic, probably as consequence of continent–continent collision during amalgamation of the supercontinent Rodinia.

The kinematic reconstruction for the continental collision phase at the end of the Mesoproterozoic is now less certain than apparent from previous literature (e.g. Groenewald et al., 1995), since the main deformation, top-to-northwest thrusting (D_2), has been re-interpreted as being Pan-African in age. The available information on the regional distribution of M_1 mineral assemblages is insufficient to establish a metamorphic field gradient for that time, but remnants of granulite-facies mineral assemblages are now known from the Heimefrontfjella, the H. U. Sverdrupfjella and the eastern Gjelsvikfjella.

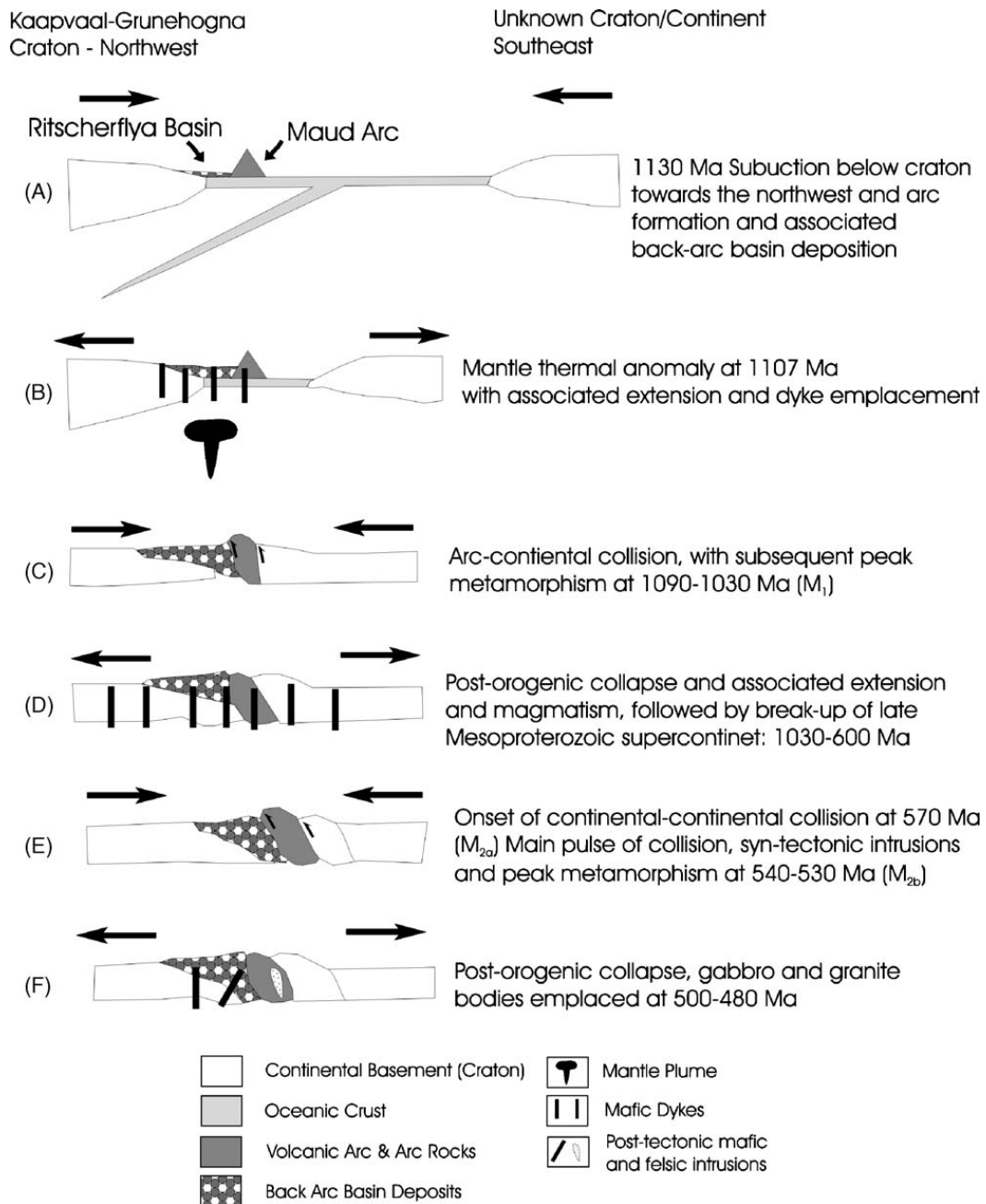


Fig. 7. Schematic diagram of the crustal evolution of western Dronning Maud Land from a Gjelsvikfjella perspective.

The rocks of the Gjelsvikfjella area were overprinted by a second high-grade tectono-metamorphic event. The peak metamorphic mineral assemblage and fabric forming (S_2) minerals are identical to those in H.U. Sverdrupfjella for which a Pan-African age has been established (Board et al., 2005). By analogy, the same age for the main tectonic fabric of the study area is inferred. Consequently the various age data obtained in this study on metamorphic zircon overgrowths are interpreted as reflecting a major Pan-African tectono-thermal overprint between 540 and 530 Ma.

An ophiolite complex preserved in the northern Shackleton Range of presumably post-Grenvillian age (Talarico et al., 1999) suggests that an ocean separated the Kalahari Craton from the East Antarctic Craton (Tessensohn et al., 1999) sometime between 1030 and 600 Ma. This ocean was progressively closed by subduction (e.g. Tessensohn et al., 1999) with the onset of continental–continental collision at ca. 570 Ma and the main pulse of collision and syn-tectonic intrusions followed by peak metamorphism between 540 and 530 Ma. Recently published data by Schmädicke and Will (2006) reveal that mafic to ultramafic rocks in the northern

Shackleton Range experienced eclogite-facies metamorphism during Pan-African orogeny. A similar scenario is now established also for the Maud Belt, but there is no evidence of juvenile Neoproterozoic crust has so far been discovered. Thus, the question of the location of the suture between the Kaapvaal-Grunehogna Craton and the East Antarctic Craton, possibly representing the boundary between East- and West-Gondwana, remains unresolved.

The penetrative S_2 fabric in the Gjelsvikfjella area has been affected by both the D_3 and D_4 events, which produced large-scale open folds thereby re-orientating the pervasive fabric locally. These open folds are interpreted to be dome structures that have accommodated the emplacement of voluminous late- to post-orogenic igneous bodies that occur in the northern and eastern Gjelsvikfjella.

In central Dronning Maud Land, H.U. Sverdrupfjella and Gjelsvikfjella, crustal thickening began at approximately 570 Ma with a maximum reached at approximately 540 Ma. This was followed by a phase of extension, which was accompanied by diverse syn-tectonic (relative to the extensional phase) magmatism. In central Dronning Maud Land, the syn-tectonic magmatism is characterised by A-type granitoids, charnockite and gabbro which has been dated at 527 ± 5 Ma and interpreted to represent a phase of late-orogenic collapse followed by post-tectonic (512–490 Ma) magmatism (Jacobs et al., 2003c). The latter is particularly evident in the Gjelsvikfjella area, where bimodal magmatism, probably induced by partial decompression-melting of the uppermost mantle and lower crust, is indicated by the 487 ± 4 Ma Stabben metagabbro and syenite. Further re-heating of the crust at that stage is also evidenced by the younger, contemporaneous zircon overgrowths established in this study (Table 9).

7. Conclusions

The U–Pb SHRIMP zircon ages obtained in this study show that Gjelsvikfjella was part of a Pan-African orogenic belt that can be traced to H.U. Sverdrupfjella (Board et al., 2005) in the west and central Dronning Maud Land (Jacobs et al., 1998) in the east. Within this belt, a ca. 1130 Ma Mesoproterozoic volcanic arc and possibly remnants of a back-arc fill became reworked, once during continental collision at the end of the Mesoproterozoic (ca. 1070 Ma) and again during Pan-African orogeny with a first stage of dynamic recrystallisation at approximately 565 Ma, peak of metamorphism reached at 530 Ma and orogenic collapse-induced bimodal magmatism between 480 and 500 Ma.

Volcanic arc formation in the Maud Belt seems not to be connected with the formation of oceanic island arcs along the southern margin of the Kaapvaal Craton (Natal sector of Namaqua-Natal Belt), but occurred later and as consequence of inboard subduction beneath the Kaapvaal-Grunehogna Craton, with the Ritscherflya Supergroup having been deposited in a back-arc position. Contiguity between the Maud Belt and the Namaqua-Natal Belt was only achieved at the end of the Mesoproterozoic when both formed part of a possibly global suture in the amalgamation of a supercontinent.

Similarity in tectonic, kinematic and metamorphic history between the Maud Belt and the Mozambique Belt (East African Orogen; e.g. Grunow et al., 1996; Sacchi et al., 1998; Manhica et al., 2001) points to both having formed a contiguous unit at the end of the Neoproterozoic. No evidence of juvenile Neoproterozoic crust has been discovered so far in the Maud Belt. This may be due to the Maud Belt taking a more central position in the East African Orogen and its continuation into East Antarctica relative to the Shackleton Range. The latter would have been in a marginal position that was never affected by the same extent of crustal thickening because of lateral escape during continent–continent collision. The abundance of late to post-tectonic magmatic rocks in the Maud Belt is explained by the intrusion of hot asthenospheric mantle following the delamination of the root of the thickened orogen in the transition zone between the central and the marginal (southernmost) part of the orogen as suggested by Jacobs et al. (2003b).

Acknowledgements

G. Doyle and C. Jackson are thanked for their field support and companionship during the Antarctic field seasons. E. Grosch is thanked for his assistance in the field. S. McCourt is thanked for his helpful input and advice to an earlier version of this manuscript. Critical comments from I.C.W. Fitzsimons and an anonymous reviewer improved an earlier version of the manuscript. A constructive review from A.S. Collins helped to shape the final product. C. Jackson and G. Viola are thanked for their input into discussions on the structural geology of the area. M. Waldron assisted with the acquisition of cathodoluminescence images and A. Spath assisted with REE analyses on the LA-ICPMS. This project was funded by a grant through the South African National Antarctic Programme (Department of Environmental Affairs and Tourism) to H.E. Frimmel. Additional funds were obtained from The Trans-Antarctica Association (TAA) to A. Bisnath.

Appendix A. Rare earth element concentrations of individual zircon domains

Sample	La	Ce	Pr	Nd	Sm	Eu	Gd	Tb	Dv	Ho	Er	Tm	Yb	Lu
ABA10A-17rim	1.06	21.81	1.49	13.04	12.32	0.63	55.32	22.05	233.37	78.54	299.64	55.86	457.26	86.10
ABA10A-18rim	1.59	15.49	0.86	5.50	7.80	0.46	36.73	13.79	173.70	65.52	300.14	65.30	614.40	120.45
ABA10A-19Acore	15.95	198.52	17.25	105.49	43.94	15.35	85.89	25.84	266.50	88.15	349.23	67.49	580.39	107.98
ABA10A-19Bcore	18.11	189.94	17.51	99.68	54.25	8.28	137.29	41.19	416.57	137.00	533.53	101.95	864.43	155.98
ABA10A-21core	15.71	105.14	7.88	43.56	21.67	4.26	63.01	22.89	280.89	106.86	480.94	103.57	978.22	195.95
ABA10A-23Arim	1.37	11.91	0.84	7.16	11.64	0.20	67.52	29.90	365.62	138.29	611.40	125.37	1069.03	202.83
ABA10A-23Brim	0.85	19.27	1.05	6.60	8.43	0.39	48.75	21.72	274.41	106.19	480.43	100.15	904.27	162.62
ABA10B-2core	1.80	6.58	0.67	3.10	7.57	0.22	45.52	20.32	252.49	96.56	432.61	89.80	776.89	150.28
ABA10B-3core	2.22	9.43	0.76	5.29	9.20	0.22	53.34	23.22	291.10	109.11	470.29	95.35	852.53	159.61
ABA81-36rim	21.71	120.27	9.25	61.69	22.32	4.12	35.68	7.71	73.85	21.20	103.47	25.01	279.39	74.41
ABA81-37rim	18.30	130.04	8.63	52.69	20.89	5.26	36.12	8.03	71.40	24.79	114.14	28.19	254.08	56.85
ABA81-43Acore	38.64	220.38	19.34	109.60	38.71	9.64	64.40	11.30	91.49	28.25	112.10	22.54	222.36	49.98
ABA81-43Bcore	43.25	193.69	19.83	114.54	40.97	8.95	43.29	8.84	69.91	22.95	107.25	25.52	298.29	74.96
ABA81-44rim	17.25	143.17	11.04	64.40	31.59	6.70	44.53	10.60	99.23	31.76	137.69	31.60	324.40	70.88
WBJS#16core	8.81	59.56	3.61	13.94	4.28	0.92	13.93	3.97	39.69	15.48	76.84	15.89	174.07	40.08
WBJS#16rim	1.44	7.09	0.59	3.31	1.19	0.23	2.91	0.62	6.52	3.18	17.15	4.40	56.02	15.88

References

- Arima, M., Tani, K., Kawate, S., Johnston, S.T., 2001. Geochemical characteristics and tectonic setting of metamorphosed rocks in the Tugela terrane, Natal belt, South Africa. *Memoirs of National Institute of Polar Research*, vol. 55, pp. 1–39.
- Arndt, N.T., Todt, W., Chauvel, C., Tapfer, M., Weber, K., 1991. U–Pb zircon age and Nd isotopic composition of granitoids, charnokites and supracrustal rocks from Heimefrontfjella, Antarctica. *Geol. Rundschau* 80, 759–777.
- Bauer, W., Thomas, R.J., Jacobs, J., 2003a. Proterozoic–Cambrian history of Dronning Maud Land in the context of Gondwana assembly. In: Yoshida, M., Windley, B.F., Dasgupta, S. (Eds.), *Proterozoic East Gondwana: Supercontinent Assembly, Breakup*. Geological Society London, Special Publication, pp. 206, 247–269.
- Bauer, W., Jacobs, J., Fanning, C.M., Schmidt, R., 2003b. Late Mesoproterozoic arc and back-arc volcanism in the Heimefrontfjella (East Antarctica) and implications for the Palaeogeography at the southeastern margin of the Kaapvaal–Grunehogna Craton. *Gondwana Res.* 6, 449–465.
- Basson, I.J., Perritt, S., Watkeys, M.K., Menzies, A.H., 2004. Geochemical correlation between metasediments of the Mfongosi Group of the Natal Sector of the Namaqua–Natal Metamorphic Province, South Africa and Ahlmannryggen Group of the Grunehogna Province, Antarctica. *Gondwana Res.* 7, 57–73.
- Bisnath, A., Frimmel, H.E., 2005. Metamorphic evolution of the Maud Belt: P–T–t path for high-grade gneisses in Gjelsvikfjella, Dronning Maud Land, East Antarctica. *J. Afr. Earth Sci.* 43, 505–524.
- Board, W.S., Frimmel, H.E., Armstrong, R.A., 2005. Pan-African tectonism in the western Maud Belt: P–T–t path for high-grade gneisses in the H.U. Sverdrupfjella, East Antarctica. *J. Petrol.* 46, 671–699.
- Collins, A.S., Pisarevsky, S.A., 2005. Amalgamating eastern Gondwana: the evolution of the Circum-Indian Orogens. *Earth Sci. Rev.* 71, 229–270.
- Compston, W., Williams, I.S., Kirschvink, J.L., Zhang, Z., Ma, G., 1992. Zircon U–Pb ages for the early Cambrian time-scale. *J. Geol. Soc. Lond.* 149, 171–184.
- Cornell, D.H., Thomas, R.J., Bowring, S.A., Armstrong, R.A., Grantham, G.H., 1996. Protolith interpretation in metamorphic terranes: a back-arc environment with Besshi-type base metal potential for the Quha formation, Natal Province, South Africa. *Precambrian Res.* 77, 243–271.
- Dalziel, I.W.D., 1997. Neoproterozoic–Palaeozoic geography and tectonics: review, hypothesis and environmental speculation. *Geol. Soc. Am. Bull.* 109, 16–42.
- Frimmel, H.E., 2004. Formation of a late Mesoproterozoic supercontinent: the South Africa–East Antarctica connection. In: Eriksson, P.G., Altermann, W., Nelson, D.R., Mueller, W.U., Catuneanu, O. (Eds.), *The Precambrian Earth: Tempos and Events*. Elsevier, Amsterdam, pp. 240–255.
- Gose, W.A., Dalziel, I.W.D., Helper, M.A., Hutson, F., Connelly, J., 1997. Paleomagnetic data and U–Pb isotopic age determinations from Coats Land, Antarctica: implications for late Proterozoic reconstructions. *J. Geophys. Res.* 102 (B4), 7887–7902.
- Grantham, G.H., Jackson, C., Moyes, A.B., Groenewald, P.B., Harris, P.D., Ferrar, G., Krynanuw, J.R., 1995. The tectonothermal evolution of the Kirwanveggen–H.U. Sverdrupfjella area, Dronning Maud Land, Antarctica. *Precambrian Res.* 75, 209–229.
- Groenewald, P.B., Grantham, G.H., Watkeys, M.K., 1991. Geological evidence for a Proterozoic to Mesozoic link between southeastern Africa and Dronning Maud Land, Antarctica. *J. Geol. Soc. Lond.* 148, 1115–1123.
- Groenewald, P.B., Hunter, D.R., 1991. Granulites of the northern H.U. Sverdrupfjella, western Dronning Maud Land: metamorphic history from garnet–pyroxene assemblages, coronas and hydration reactions. In: Thomson, M.R.A., Crame, J.A., Thomson, J.W. (Eds.), *Geological Evolution of Antarctica*. Cambridge University Press, Cambridge, pp. 61–66.
- Groenewald, P.B., Moyes, A.B., Grantham, G.H., Krynanuw, J.R., 1995. East Antarctic crustal evolution: geological constraints and modelling in western Dronning Maud Land. *Precambrian Res.* 75, 231–250.
- Grosch, E.G., Bisnath, A., Frimmel, H.E., Board, W.S., 2004. Geochemistry and Tectonic setting of Proterozoic Mafic Rocks in Western Dronning Maud Land, Antarctica. *Geoscience Africa*

2004. Abstract Volume, University of Witwatersrand, Johannesburg, South Africa, pp. 229–230.
- Grunow, A., Henson, R., Wilson, T., 1996. Were Aspects of the Pan-African deformation linked to Iapetus opening? *Geology* 24, 1063–1066.
- Hanson, R.E., Martin, M.W., Bowring, S.A., Munyanyiwa, H., 1998. U–Pb zircon age for the Umkondo dolerites, eastern Zimbabwe: 1.1 Ga large igneous province in southern Africa-East Antarctica and possible Rodinia correlations. *Geology* 26, 1143–1146.
- Hanson, R.E., Crowley, J.L., Bowring, S.A., Ramezani, J., Cose, W.A., Dalziel, I.W.D., Pancake, J.A., Seidel, E.K., Blenkinsop, Thomas, G., Mukwakwami, J., 2004. Coeval large-scale magmatism in the Kalahari and Laurentian Cratons during Rodinia assembly. *Science* 304, 1126–1129.
- Harris, P.D., Moyes, A.B., Fanning, C.M., Armstrong, R.A., 1995. Zircon ion microprobe results from the Maudheim high-grade gneiss terrane, western Dronning Maud Land, Antarctica: Centennial Geocongress (1995). Johannesburg, pp. 240–243.
- Harris, P.D., 1999. The geological evolution of Neumayerskarvet in the Northern Kirwanveggen, Western Dronning Maud Land, Antarctica. Unpublished Ph.D. thesis, Rand Afrikaans University, Johannesburg.
- Hoffman, P.F., 1991. Did the breakout of Laurentia turn Gondwana inside-out? *Science* 252, 1409–1412.
- Jackson, C., 1999. Characterization of Mesoproterozoic to Palaeozoic crustal evolution of western Dronning Maud Land. Study 3: Deformational history and thermochronology of the central Kirwanveggen. Unpublished report, Department of Environmental Affairs and Tourism, Pretoria, p. 80.
- Jacobs, J., Thomas, R.J., Weber, K., 1993. Accretion and indentation tectonics at the southern edge of the Kaapvaal craton during the Kibaran (Grenville orogen). *Geology* 21, 203–206.
- Jacobs, J., Thomas, R.J., 1994. Oblique collision at about 1.1 Ga along the southern margin of the Kaapvaal continent, south-east Africa. *Geol. Rundschau* 83, 322–333.
- Jacobs, J., Bauer, W., Spaeth, G., Thomas, R.J., Weber, K., 1996. Lithology and structure of the Grenville-aged (1.1 Ga) basement of Heimfrontjella (East Antarctica). *Geol. Rundschau* 85, 800–821.
- Jacobs, J., Fanning, C.M., Henjes-Kunst, F., Olesch, M., Paech, H.-J., 1998. Continuation of the Mozambique Belt into East Antarctica: Grenville-age metamorphism and polyphase Pan-African high-grade events in central Dronning Maud Land. *J. Geol.* 106, 385–406.
- Jacobs, J., Hansen, B.T., Henjes-Kunst, F., Thomas, R.J., Bauer, W., Weber, K., Armstrong, R.A., Cornell, D.H., 1999. New age constraints on Proterozoic/lower Palaeozoic evolution of Heimfrontjella, East Antarctica, and its bearing on Rodinia/Gondwana correlations. *Terra Antarctica* 6, 377–389.
- Jacobs, J., Fanning, C.M., Bauer, W., 2003a. Timing of Grenville-age vs Pan-African medium- to high-grade metamorphism in western Dronning Maud Land (East Antarctica) and significance for correlations in Rodinia and Gondwana. *Precambrian Res.* 125, 1–20.
- Jacobs, J., Bauer, W., Fanning, C.M., 2003b. Late Neoproterozoic/Early Palaeozoic events in central Dronning Maud Land and significance for the southern extension of the East African Orogen into East Antarctica. *Precambrian Res.* 126, 27–53.
- Jacobs, J., Klemd, R., Fanning, C.M., Bauer, W., Colombo, F., 2003c. Extensional collapse of the late Neoproterozoic-early Palaeozoic East African-Antarctic Orogen in central Dronning Maud Land, East Antarctica. In: Yoshida, M., Windley, B.F., Dasgupta, S. (Eds.), *Proterozoic East Gondwana: Supercontinent Assembly and Breakup*, Geological Society, London. Special Publication, pp. 206, 271–285.
- Jacobs, J., Bauer, W., Fanning, C.M., 2003d. New age constraints for Grenvillian age metamorphism in western central Dronning Maud Land (East Antarctica), and implications for the palaeogeography of Kalahari in Rodinia. *Int. J. Earth Sci. (Geol. Rundschau)* 92, 301–315.
- Johnston, S.T., Armstrong, R., Heaman, L., McCourt, S., Mitchell, A., Bisnath, A., Arima, M., 2001. Preliminary U–Pb geochronology of the Tugela terrane, Natal belt, eastern South Africa. *Memoirs of National Institute of Polar Research*, vol. 55, pp. 40–58.
- Krynauw, J.R., 1996. A review of the geology of east Antarctica, with special reference to the c. 1000 Ma and c. 500 Ma events. *Terra Antarctica* 3, 77–89.
- Ludwig, K.R., 1999. User's Manual for Isoplot/Ex, Version 2.10, A Geochronological Toolkit for Microsoft Excel. Berkeley Geochronology Center Special Publication, Berkeley, USA.
- Ludwig, K.R., 2000. SQUID 1.00, User's Manual. Berkeley Geochronology Center Special Publication, Berkeley, USA.
- Manhica, A.S.T.D., Grantham, G.H., Armstrong, R.A., Guise, P.G., Kruger, F.J., 2001. Polyphase deformation and metamorphism at the Kalahari Craton-Mozambique Belt boundary. In: Miller, J.A., Holdsworth, R.E., Buick, I.S., Hand, M. (Eds.), *Continental Reactivation and Reworking*. Geological Society of London, pp. 184, 303–321.
- Meert, J.G., 2003. A synopsis of events related to the assembly of Eastern Gondwana. *Tectonophysics* 362, 1–40.
- Moyes, A.B., Krynauw, J.R., Barton, J.M., 1995. The age of the Ritscherflya Supergroup and Borgmassivet intrusions, Dronning Maud Land (Antarctica). *Antarctic Sci.* 7, 87–97.
- Moyes, A.B., Groenewald, P.B., 1996. Isotopic constraints on Pan-African metamorphism in Dronning Maud Land, Antarctica. *Chem. Geol.* 129, 247–256.
- Ohta, Y., Tørudbakken, B.O., 1985. Geology of the Gjelsvikfjella and western Mühlig-Hoffmannfjella, western Dronning Maud Land, East Antarctica. In: Orheim, O. (Ed.), *Report of Norwegian Antarctic Research Expedition (NARE 1984/85)*. Norwegian Polar Institute Report Series, Oslo, pp. 35–41.
- Ohta, Y. (Ed.), 1999. Nature Environment Map, Dronning Maud Land, Gjelsvikfjella and western Mühlig-Hofmannfjella 1:100,000. Norsk Polarinst. TEMAKART, Nr. 24, 1999.
- Paces, J.B., Miller, J.D., 1993. Precise U–Pb ages of Duluth Complex and related mafic intrusions, Northeastern Minnesota: geochronological insights to physical, petrogenic, and paleomagnetic and tectonomagnetic processes associated with the 1.1 Ga mid-continent rift system. *J. Geophys. Res.* 98B, 13997–14013.
- Paulsson, O., Austrheim, H., 2003. A geochronological and geochemical study of rocks from Gjelsvikfjella, Dronning Maud Land, Antarctica-implications for Mesoproterozoic correlations and assembly of Gondwana. *Precambrian Res.* 125, 113–138.
- Raith, J.G., Cornell, D.H., Frimmel, H.E., de Beer, C.H., 2003. New insights into the geology of the Namaqua Tectonic Province, South Africa, from ion probe dating of detrital and metamorphic zircon. *J. Geol.* 111, 347–366.
- Ramsay, J.G., 1967. *Folding and Fracturing of Rocks*. McGraw-Hill, New York, p. 567.
- Reeves, C., de Wit, M.J., 2000. Making ends meet in Gondwana: retracing the transforms of the Indian Ocean and reconnecting continental shear zones. *Terra Nova* 12, 272–280.
- Robb, L.J., Armstrong, R.A., Waters, D.J., 1999. The history of granulite-facies metamorphism and crustal growth from single zir-

- con U–Pb geochronology: Namaqualand, South Africa. *J. Petrol.* 40, 1747–1770.
- Sacchi, R., Cadoppi, P., Costa, M., 1998. The relationship between the Lurio Belt and the Mozambique. In: Almond, J., Anderson, J., Booth, P., Chinsamy-Turan, A., Cole, D., DeWit, M.J., Rubridge, B., Smith, R., van Bever Donker, J., Storey, B.C. (Eds.), *Gondwana 10: Event Stratigraphy of Gondwana (abstracts)*, 28th June to 5th July 1998. Cape Town, *Journal of African Earth Science*. 27, 165.
- Schmädicke, E., Will, T.M., 2006. First evidence for eclogite facies metamorphism in the Shackleton Range, Antarctica: trace of suture between East and West Gondwana. *Geology* 34, 133–136.
- Shelley, D., 1983. *Igneous and Metamorphic Rocks under the Microscope: Classification, Texture, Microstructures and Mineral Preferred-Orientations*. Chapman and Hall, London, p. 445.
- Sun, S., McDonough, W.F., 1989. Chemical and isotopic systematics of ocean basalts: implications for mantle composition and processes. In: Saunders, A.D., Norry, M.J. (Eds.), *Magmatism in the Ocean Basins*. Geological Society London, London, pp. 313–345.
- Talarico, F., Kleinschmidt, G., Henjes-Kunt, F., 1999. An ophiolite complex in the northern Shackleton range, Antarctica. *Terra Antarctica* 6, 317–325.
- Tera, F., Wasserburg, G., 1972. U–Th–Pb systematics in three Apollo 14 basalts and the problem of initial Pb in lunar rocks. *Earth Planet. Sci. Lett.* 14, 281–304.
- Tessensohn, F., Kleinschmidt, G., Talarico, F., Buggisch, W., Brommer, A., Henjes-Kunst, F., Kroner, U., Millar, I.L., Zeh, A., 1999. Ross-age amalgamation of East and West Gondwana: evidence from the Shackleton Range, Antarctica. *Terra Antarctica* 6, 317–325.
- Thomas, R.J., Cornell, D.H., Armstrong, R.A., 1999. Provenance age and metamorphic history of the Quha Formation, Natal Metamorphic Province: a U–Th–Pb zircon SHRIMP study. *S. Afr. J. Geol.* 102, 83–88.
- Tingey, R.J., 1991. The regional geology of Archaean and Proterozoic rocks in Antarctica. In: Tingey, R.J. (Ed.), *The Geology of Antarctica*. Oxford University Press, Oxford, pp. 1–73.
- Wingate, M.T.D., Pirajno, F., Morris, P.A., 2004. The Warakurna large igneous province: a new Mesoproterozoic large igneous province in west-central Australia. *Geology* 32, 105–108.
- Williams, I.S., 1998. U–Th–Pb geochronology by ion microprobe. In: McKibben, M.A., Shanks III, W.C., Ridley, W.I. (Eds.), *Applications of Microanalytical Techniques to Understanding Mineralizing Processes*. *Reviews in Economic Geology*. 7, 1–35.
- Williams, I.S., Claesson, S., 1987. Isotopic evidence for the Precambrian provenance and Caledonian metamorphism of high grade paragneisses from the Seve nappes, Scandanavian Caledonides. II. Ion microprobe zircon U–Th–Pb. *Contrib. Mineral. Petrol.* 97, 205–217.
- Wolmarans, L.G., Kent, L.E., 1982. Geological investigations in Western Dronning Maud Land, Antarctica—a synthesis. *S. Afr. J. Antarctic Res.* 2, 93.